

A framework for deep energy-based reinforcement learning with quantum speed-up

Sofiene Jerbi,¹ Hendrik Poulsen Nautrup,¹ Lea M. Trenkwalder,¹ Hans J. Briegel,^{1,2} and Vedran Dunjko³

¹*Institute for Theoretical Physics, University of Innsbruck, Technikerstr. 21a, A-6020 Innsbruck, Austria*

²*Department of Philosophy, University of Konstanz, Fach 17, 78457 Konstanz, Germany*

³*LIACS, Leiden University, Niels Bohrweg 1, 2333 CA Leiden, The Netherlands*

(Dated: November 11, 2021)

In the past decade, deep learning methods have seen tremendous success in various supervised and unsupervised learning tasks such as classification and generative modeling. More recently, deep neural networks have emerged in the domain of reinforcement learning as a tool to solve decision-making problems of unprecedented complexity, e.g., navigation problems or game-playing AI. Despite the successful combinations of ideas from quantum computing with machine learning methods, there have been relatively few attempts to design quantum algorithms that would enhance deep reinforcement learning. This is partly due to the fact that quantum enhancements of deep neural networks, in general, have not been as extensively investigated as other quantum machine learning methods. In contrast, projective simulation is a reinforcement learning model inspired by the stochastic evolution of physical systems that enables a quantum speed-up in decision making. In this paper, we develop a unifying framework that connects deep learning and projective simulation, opening the route to quantum improvements in deep reinforcement learning. Our approach is based on so-called generative energy-based models to design reinforcement learning methods with a computational advantage in solving complex and large-scale decision-making problems.

I. INTRODUCTION

The advent of deep learning [1] is responsible for many of the outstanding achievements in supervised and unsupervised learning over the past decade. Deep neural networks have found a wide range of applications in various data-abundant problems: starting from the multilayer perceptron for general classification and regression tasks, convolutional neural networks [2] quickly became the reference in computer vision, and generative adversarial networks [3] are today’s state-of-the-art generative models.

Besides supervised and unsupervised learning, reinforcement learning (RL) [4] is the third paradigm of machine learning. While both supervised and unsupervised learning aim at learning fixed (conditional) probability distributions from independent and identically generated samples, RL focuses on learning from interaction in sequential decision-making problems such as control or planning. More specifically, the objective of RL is to learn an optimal behavior (or policy) from a scalar reward signal that is generally sparse, delayed and dependent on this policy. The theory of RL has its roots in mathematical optimization literature, and more especially the work of Bellman on dynamic programming [5] from which the so-called *value-based methods* such as SARSA and *Q-learning* [4] originated. A long-existing open problem in RL was to exhibit successful generalization abilities in an interactive learning scenario, analogously to the breakthroughs of deep learning in (un)supervised learning. In RL, generalization amounts for the ability to learn what action to take in *similar* scenarios (which entails learning a notion of similarity) and is particularly relevant in task environments with large state and action spaces, e.g., the board game of Go has a state space of size 10^{172} .

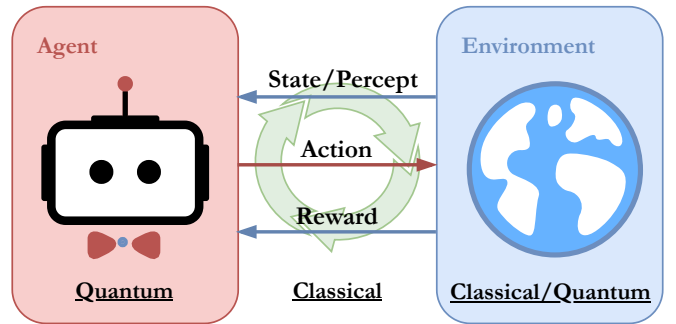


Figure 1. **Quantum-enhanced reinforcement learning.** Agent and environment maintain a cyclic interaction consisting of *states* (or *percepts*) that the agent uses to deliberate on its *actions* according to its policy, and perceives feedback on its behavior in the form of *rewards*. In the quantum-enhanced framework, the agent is granted access to a, generally universal, quantum computer to enhance its deliberation process.

Due to a potential instability in learning, RL has been widely believed, until recently, to be incompatible with deep learning methods [6]. However, a recent breakthrough by Mnih et al. [7] gave rise to a new entire branch of RL – deep reinforcement learning [8] – whose distinctive addition to the field is the ability to learn good policies in task environments characterized by high-dimensional spaces. Most notably, deep RL agents can achieve (super)human-level performance in complex games such as Atari [7], chess [9] and Go [10] or in complex cognitive tasks such as city navigation in “first-person view” [11].

Concurrently to the developments of deep RL, we have witnessed significant strides in the domain of quantum machine learning with the emergence of various quan-

tum algorithms efficiently solving problems mostly in supervised and unsupervised learning [12–16]. In the field of quantum reinforcement learning [17], promising speed-ups in learning efficiency have been demonstrated for RL agents in quantum-accessible environments, i.e., when agent and environment are able to maintain a quantum interaction [18–20]. However, barring a few recent works [21–24] that we partially discuss in Sec. V, quantum enhancements of classical approaches to RL – and especially the highly successful deep RL methods – have been mostly overlooked by the quantum machine learning community. A notable exception to this line of research is projective simulation (PS) [25], a recently introduced model for the design of learning agents inspired by the stochastic evolution of physical systems. Indeed, PS has been shown to benefit from a computational advantage in a quantum-enhanced scenario [26] (see Fig. 1): the algorithm that guides PS agents’ decision making is based on a random walk process whose quantum counterpart is quadratically faster [27, 28].

In this work, we propose a framework that unifies deep value-based methods and PS and allows us to design deep RL agents able to act and learn more efficiently within environments having large state and action spaces. To this end, we build on a physical approach to neural networks – so-called energy-based models [29] – and link the inference process over these models to the random walk deliberation in PS. This approach benefits from the tools and intuition of both methods and gives rise to agents with expressive policies leveraged by a quantum speed-up in deliberation.

The paper is organized as follows: Sec. II serves as an introduction to the long-studied problem of large state and action spaces in reinforcement learning and the (in)adequacy of different methods to deal with this issue; Sec. III presents a step-by-step construction of the deep energy-based networks we consider, where each addition to the model allows us to learn in environments with increasing complexity, as the numerical simulations presented in that section suggest; Sec. IV describes random walk algorithms that allow for faster deliberation using these deep energy-based networks and explains how quantum algorithms can further speed-up these random walks; Sec. V lists related work and Sec. VI is reserved for discussion.

II. BACKGROUND & OVERVIEW

In this section, we introduce the well-studied case of reinforcement learning environments with large state and action spaces and discuss modern approaches [7, 30] that attempt to deal with such scenarios by contrasting them with traditional RL methods [4, 25].

Overview		
Agent's ability	Feature	Section
Generalization	• Neural networks	II.B
Multimodal representations	• Energy-based models	III.A
Representational power	• Deep neural networks	III.B
Deliberation in large action spaces	• Approximate sampling methods • Speed-up via quantum walks	IV

Figure 2. Quantum deep energy-based agents

A. Tabular methods

Reinforcement learning (RL) is a framework for the design of learning agents in interactive environments (see Fig. 1). Typically, the goal of RL is to learn a policy $\pi(\mathbf{a}|\mathbf{s})$ that guides an agent’s actions \mathbf{a} given a perceived state \mathbf{s} towards maximizing its future rewards in a certain environment. There exist various approaches to learn optimal policies. However, in this work, we focus on two particular methods that we combine in a unifying framework. This framework allows us to combine and take advantage of their respective techniques and previous work. We give here a short description of the two methods of interest, further detailed in Appendix A:

- Methods deriving from dynamic programming focus on a so-called *action-value function* $Q(\mathbf{s}, \mathbf{a})$ to link policy and expected rewards. These *value-based methods* (VBMs) include, for instance, Q -learning and SARSA.
- Projective simulation (PS) is a physically-inspired model for agency¹ that relies on weighted connections in a directed graph to reflect experienced rewards and derive a policy. These weights are referred to as h -values. In its simplest (i.e., two-layered) form, the underlying weighted graph only contains directed connections from states to actions, resulting in state-action h -values $h(\mathbf{s}, \mathbf{a})$.

¹Note that, in standard VBMs, states and actions are part of a mathematical object describing the agent’s task environment: a Markov Decision Process. In PS, although similar to VBMs in its two-layer form, the perspective is different and more agent-centered: representations of states and actions have a separate status as entities in the agent’s memory, they can be created, erased, or modified as part of the agent’s dynamics of memory processing and deliberation.

In our effort to unify these two approaches, we define the notion of *merit functions* M , of which both auxiliary functions Q and h are instances. These are real-valued functions defined on the state-action space that assign a certain value of merit to all actions in any given state. A standard procedure to learn merit functions and their associated policies is the so-called *tabular* method, which is shared by both VBMs and two-layered PS: scalar values $\hat{M}(\mathbf{s}, \mathbf{a})$ are stored for each state-action pair, initialized such as to produce a random behavior. These can be normalized into a policy, e.g., by using a Gibbs/Boltzmann distribution,

$$\pi(\mathbf{a}|\mathbf{s}) = \frac{e^{\beta \hat{M}(\mathbf{s}, \mathbf{a})}}{\sum_{\mathbf{a}'} e^{\beta \hat{M}(\mathbf{s}, \mathbf{a}')}} \quad (1)$$

where $\beta > 0$ is an inverse temperature hyperparameter. An update rule given by VBMs or PS allows one to iteratively update the values $\hat{M}(\mathbf{s}, \mathbf{a})$ associated with *experienced* state-action pairs. This update depends on the rewards received from the environment after following this policy and increases the estimated merit value of rewarded state-action pairs such that the agent is more likely to encounter them in the future. For instance, in the case of Q -learning (which is a VBM):

$$\hat{Q}(\mathbf{s}^{(t)}, \mathbf{a}^{(t)}) \leftarrow (1 - \alpha) \hat{Q}(\mathbf{s}^{(t)}, \mathbf{a}^{(t)}) + \alpha [r^{(t+1)} + \gamma \max_{\mathbf{a}} \hat{Q}(\mathbf{s}^{(t+1)}, \mathbf{a})] \quad (2)$$

where $\mathbf{a}^{(t)}$ is the action performed by the agent in the state $\mathbf{s}^{(t)}$ at timestep t , which lead it to the state $\mathbf{s}^{(t+1)}$ and associated reward $r^{(t+1)}$; α is a learning rate taking value in $[0, 1]$ and used to deal with statistical fluctuations.

The fundamental problem with tabular approaches is their lack of generalization capabilities: there is no mechanism enabling an agent to generalize learned values to unobserved states and actions. This puts a strong lower bound on the number of interactions with the environment required to learn an optimal merit function: $\Omega(|\mathcal{S}| \times |\mathcal{A}|)$. That is, the number of interactions scales at least linearly in the number of state-action pairs [21]². Hence, learning through tabular methods becomes intractable for environments with large (potentially continuous) state and action spaces. However, this is a rather common aspect of practical RL tasks:

- Large (and continuous) state spaces appear, for instance, when the sensory input of an agent includes images, as the dimension of its state space grows linearly with their number of pixels.

- Large action spaces are common for recommender systems such as YouTube or Netflix, where the actions are the possible recommendations of contents that can be made to a user. They also appear in many control problems of large processes, including, for instance, quantum control and quantum experiments [31–41]. For tasks such as these, actions are characterized by continuous parameters that are commonly discretized to efficiently search for their optimal values. The drawback of this approach is that the action space grows polynomially with the inverse precision of discretization ε^{-1} . More precisely, the size of the action space is $(\frac{L}{\varepsilon})^d$, where L is the range of the d continuous action parameters.

B. Generalization with neural networks

A common way to provide RL agents with generalization mechanisms is through *function approximation* methods. Such approaches introduce a parameterized representation $M^\theta(\mathbf{s}, \mathbf{a})$ of the merit function, replacing an otherwise sparsely-filled merit table by a function that is defined on the entire state-action space. Updates of the merit function act no longer on individual values $\hat{M}(\mathbf{s}, \mathbf{a})$ but on a set of parameters θ , allowing one to indirectly update the values $M^\theta(\mathbf{s}, \mathbf{a})$ of many – including unobserved – state-action pairs simultaneously. Using the terminology of supervised learning, $\{M^\theta\}_\theta$ constitutes the set of all possible hypothesis functions and learning consists in updating the parameters θ as to find the setting that best approximates the true merit function M . Due to their success in supervised and unsupervised learning, neural networks, parameterized by their weights, have gained popularity as function approximators in RL. While generalization over the state space is a shared feature of all function approximation methods based on neural networks, generalization over the action space, i.e., learning a useful similarity measure between actions, is less common.

When using feedforward neural networks as function approximators, one can choose between two different approaches to represent the merit function (see Fig. 3). The first representation (*i*) takes as input a state \mathbf{s} and outputs *all values* ($M^\theta(\mathbf{s}, \mathbf{a}_1), \dots, M^\theta(\mathbf{s}, \mathbf{a}_{|\mathcal{A}|})$) associated to that state; while the second (*ii*) takes as input a single state-action pair (\mathbf{s}, \mathbf{a}) and outputs its corresponding merit value $M^\theta(\mathbf{s}, \mathbf{a})$. Each of these representations has its advantages in different contexts, that we clarify below.

In their seminal work [7], Mnih et al. introduce a so-called deep Q -network (DQN) of type (*i*) that quickly became the standard in value-based deep RL [42]. DQNs are particularly successful in vision problems, e.g., playing Atari games, as their convolutional hidden layers make them perfectly suited to deal with the high-dimensional

²Note that the generalization mechanisms of the next subsection do not overcome this lower bound complexity for *general* environments. But the specificity of real-world tasks allows, through heuristic approaches, to learn much faster.

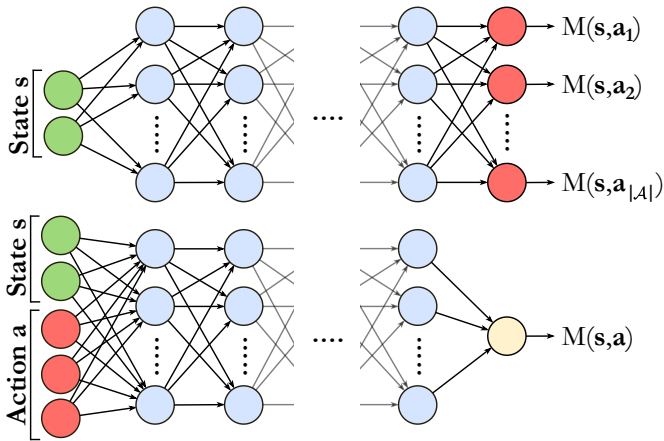


Figure 3. **A sketch of comparison between the layouts of DQN-like networks [7] and the DEBN we consider.** The first hidden layers may be convolutional.

space of the images they receive as input. Moreover, having all the merit values associated to a given state in the output layer makes it particularly efficient to evaluate the policy (1) of the agent, since it requires only a single evaluation of the neural network followed by the application of a single additional softmax layer that normalizes the output. However, this representation suffers from a serious caveat when it comes to tasks with large action spaces. During the first stages of learning, it is important for the agent to keep an explorative behavior to not get stuck in a possibly sub-optimal policy. For this reason, it may be crucial for the neural network to be able to represent a merit function that assigns, for a given state, a high value to several actions, such that its associated policy is not only peaked for a single action. Such a “multi-peaked” representation is said to be *multimodal*. Unfortunately, a neural network whose output dimension grows linearly with the size of the action space and that has a limited number of hidden layers/units is very unlikely to represent and learn a highly multimodal function in environments with large action spaces [43, 44].

We refer to representations of type (ii) as *deep energy-based networks* (DEBN) due to their interesting connection to so-called energy-based models [29]. Inspired by statistical physics, energy-based models represent a target function using the energy function of a statistical system (that can be in one of several configurations, each having a certain energy). When calculated for all configurations and normalized, this energy function gives rise to a probability distribution over all possible configurations. This is for instance the case for Boltzmann machines, introduced by Hinton & Sejnowski to model data distributions [45], which are inspired by the Ising model for spin systems [46]. Restricted Boltzmann machines (RBMs), i.e., Boltzmann machines with a further constrained set of energy functions, were the first energy-based models reportedly used in RL with

the work of Sallans & Hinton [30], followed by various extensions [43, 47–50]. Interestingly, although RBMs belong to a class of so-called stochastic recurrent neural networks, they can be expressed as feedforward neural networks of type (ii) [51] but with a single hidden layer. The DEBNs we consider are then straightforwardly obtained by adding additional hidden layers to this feedforward neural network [52]. Energy-based models are known to better represent multimodal distributions [43], which is partially due to the fact that no parts of the DEBNs have to grow linearly with the action space. Hence, being able to encode deep and multimodal representations, DEBNs are well suited for tasks with both large state and action spaces. A major drawback of DEBNs is the high cost of sampling from the policy (1): $|\mathcal{A}|$ evaluations of the network are needed to evaluate the policy exactly. *Approximate* sampling methods based on random walks, such as Gibbs sampling, exist. But Long et al. [53] showed that approximate sampling is still an NP-hard problem in the case of RBMs, an argument that can be easily generalized to DEBNs.

In this work, we exploit the connection between RBMs and feedforward neural networks to design deep and multimodal representations of merit functions in RL. We present a systematic construction of our DEBNs and show through numerical simulations how these allow dealing with environments of increasing complexity. Moreover, we ameliorate the sampling issue of DEBNs by using quantum computation to achieve a speed-up in deliberation, i.e., sampling from their policy. To be more precise, we provide a framework inspired by the work of Paparo et al. [26] that enables the application of quantum walk algorithms to speed-up approximate sampling from energy-based policies. In this way, a quadratic speed-up in decision making can be achieved, and a new perspective on the design of quantum-enhanced RL agents is obtained.

III. DEEP ENERGY-BASED RL

In this section, we give a preliminary introduction to energy-based models, on which we build upon to design our deep energy-based learning agents. We first consider RBM function approximators for RL [30] and show their advantage over tabular methods in a simple benchmarking task with a high-dimensional state space. We then present an established connection between RBMs and shallow feedforward networks [51] which allows us to consider a natural extension to a deep architecture – our so-called DEBNs – and give numerical evidence of their advantage over RBMs in tasks with complex and continuous state spaces. Besides the numerical evidence presented here, we also refer to theoretical work on the representational efficiency of RBMs and deep neural networks that supports our claims.

A. Energy-based RL

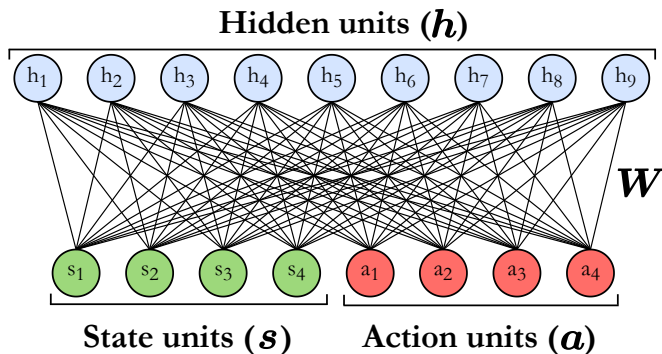


Figure 4. **A restricted Boltzmann machine used for reinforcement learning.** Biases are not represented for compactness.

Energy-based models (EBMs). EBMs are a popular class of probabilistic models that find applications in both supervised and unsupervised learning [29]. They are often used as generative models, that is, to model the empirical probability distribution of observed data vectors $\{\mathbf{v}\}_{\mathbf{v} \in \mathcal{D}}$, e.g., strings of binary variables. EBMs capture dependencies between a set of variables by assigning a scalar energy to each of their configurations, e.g., all possible binary strings of length $|\mathbf{v}|$. This energy function is usually parameterized by a vector $\boldsymbol{\theta}$ that determines the strengths of these dependencies. In the case of a Boltzmann machine, for instance, the energy function takes the form:

$$-E^\theta(\mathbf{v}) = \sum_{i < j} w_{ij} v_i v_j + \sum_i b_i v_i \quad (3)$$

and $\boldsymbol{\theta} = ((w_{ij})_{1 \leq i < j \leq |\mathbf{v}|}, (b_i)_{1 \leq i \leq |\mathbf{v}|})$ in this case. Note that this particular Boltzmann machine is said to be fully-visible, since its energy only depends on the visible variables v_i that encode the data. The topology of the model specifies which variables are presumed (in)dependent. Combined, topology and parametrization constrain the family of available energy functions $\{E^\theta\}_\theta$ that an EBM can represent.

A probability distribution over the configuration space can be derived from the energy function by a certain normalization over all possible configurations. Intuitively, normalization assigns a high probability to configurations with low energy and vice versa. This generative probability distribution can be trained, i.e., iteratively modified, to best fit an (empirical) probability distribution through updates of the parameters $\boldsymbol{\theta}$. These updates effectively select new energy functions from $\{E^\theta\}_\theta$, and, equivalently, new generative distributions.

In order to capture more complex dependencies between the *observed* variables describing the data vectors \mathbf{v} , EBMs usually introduce additional *hidden* (or *latent*) variables \mathbf{h} , such that the model has now an energy

$E^\theta(\mathbf{v}, \mathbf{h})$ that includes terms characterized by the parameters between visible and hidden variables. The probability distribution over the visible variables is then specified by a function $F^\theta(\mathbf{v})$ called the *free energy* of the model due to its connection to the equilibrium free energy in statistical physics. It is obtained by tracing out the hidden variables from the normalizing distribution. For instance, in the case of a softmax normalization:

$$P^\theta(\mathbf{v}) = \frac{\sum_{\mathbf{h}} e^{-E^\theta(\mathbf{v}, \mathbf{h})}}{\sum_{\mathbf{v}', \mathbf{h}'} e^{-E^\theta(\mathbf{v}', \mathbf{h}')}} = \frac{e^{-F^\theta(\mathbf{v})}}{\sum_{\mathbf{v}'} e^{-F^\theta(\mathbf{v}')}} \quad (4)$$

and

$$F^\theta(\mathbf{v}) = E^\theta(\mathbf{v}, \langle \mathbf{h} \rangle_{P(\mathbf{h}|\mathbf{v})}) + H(\mathbf{h}|\mathbf{v}) \quad (5)$$

where $\langle \mathbf{h} \rangle_{P(\mathbf{h}|\mathbf{v})}$ is the expectation value of the hidden variables under $P(\mathbf{h}|\mathbf{v})$ and $H(\mathbf{h}|\mathbf{v})$ is their Shannon conditional entropy under this same probability distribution. A derivation is provided in Appendix C.

Energy-based function approximation. Following the idea of Sallans & Hinton [30], we use the free energies of energy-based models as *parameterized* approximations of merit functions (such as the Q -function in VBMs [4] or the h -values of PS [25]). We start with a simple energy-based model: a restricted Boltzmann machine (RBM), further introduced in Appendix C. To represent a policy using an RBM, we divide its visible units into state and action units (see Fig. 4). This allows one to define a conditional probability distribution:

$$\pi^\theta(\mathbf{a}|\mathbf{s}) = \frac{e^{-F^\theta(\mathbf{s}, \mathbf{a})}}{\sum_{\mathbf{a}'} e^{-F^\theta(\mathbf{s}, \mathbf{a}')}} = \frac{e^{M^\theta(\mathbf{s}, \mathbf{a})}}{\sum_{\mathbf{a}'} e^{M^\theta(\mathbf{s}, \mathbf{a}')}} \quad (6)$$

effectively encoding the policy of an agent as prescribed by Eq. (1) (the inverse temperature β can be absorbed by the parameters $\boldsymbol{\theta} \rightarrow \beta\boldsymbol{\theta}$).

This approximation of the merit function by the RBM free energy, as opposed to a tabular approach, has the advantage of being defined on the entire state-action space, which allows the agent to act non-randomly on previously unseen states. Moreover, (implicitly) stored values $M^\theta(\mathbf{s}, \mathbf{a})$ are not updated independently from one another, as updates on $\boldsymbol{\theta}$ act on many values at a time, which allows one to generalize learned merit values to unobserved states and actions.

At first sight, this form of energy-based function approximation may look hard to link to an approach relying on feedforward neural networks, such as the DQN of Mnih et al. Indeed, the expression of the RBM free energy given in Eq. (5) does not seem to be expressible as a neural-network function, i.e., linear combinations of (input) variables interlaid by non-linear activation functions. But a quick derivation, deferred to Appendix C, shows that the free energy of an RBM can be evaluated *exactly* by a shallow feedforward neural network taking the form of Fig. 5. We come back to this interesting connection in the next subsection when we consider deep

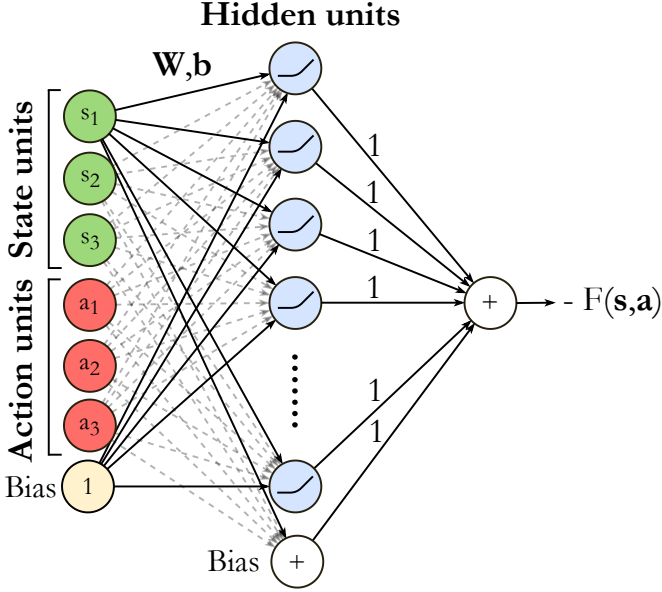


Figure 5. **A feedforward neural network computing the exact free energy of an RBM.** W and b are the vectors of weights and biases parameterizing the RBM. The activations of the hidden units are softplus functions (see Appendix C).

neural networks.

Updating the merit function. Updates on an RBM are commonly performed through gradient descent applied on the weights θ parametrizing its (free) energy. When used in an unsupervised learning scenario, the descent direction is given by the gradient of the Kullback-Leibler divergence between the RBM distribution $P^\theta(\mathbf{v})$ and the empirical data distribution $\hat{p}(\mathbf{v})$ [54]³. In a reinforcement learning scenario, however, we do not have direct access to (samples from) the optimal policy. Instead, the agent receives feedback from the environment in the form of delayed rewards. That is, feedback is given to long sequences of actions, preventing the direct evaluation of any measure of distance to the optimal policy. For this reason, the update rule of the RBM used in RL is derived from the update rule of the merit function that the model approximates. We explain this derivation in the case of Q -learning.

The original update rule [4] is given by:

$$-F^\theta(\mathbf{s}^{(t)}, \mathbf{a}^{(t)}) \leftarrow -(1 - \alpha)F^\theta(\mathbf{s}^{(t)}, \mathbf{a}^{(t)}) + \alpha[r^{(t+1)} - \gamma \max_{\mathbf{a}} F^\theta(\mathbf{s}^{(t+1)}, \mathbf{a})] \quad (7)$$

where $\hat{Q}(\mathbf{s}, \mathbf{a}) = -F^\theta(\mathbf{s}, \mathbf{a})$ in this case and $\alpha \in [0, 1]$ is the so-called learning rate. Notice that this expression is

of the form

$$\text{current} \leftarrow (1 - \alpha) \text{current} + \alpha \text{target} \quad (8)$$

where the target value is an approximation of the optimal Q -value (expressed in its bootstrapped expansion in terms of the current reward and the discounted Q -value of the next timestep) that becomes exact upon convergence to the optimal policy.

Restated differently, this update aims at decreasing the *temporal difference* error, i.e., the difference between target and current value:

$$\mathcal{E}_{\text{TD}}^\theta(t) = r^{(t+1)} - \gamma \max_{\mathbf{a}} F^\theta(\mathbf{s}^{(t+1)}, \mathbf{a}) + F^\theta(\mathbf{s}^{(t)}, \mathbf{a}^{(t)})$$

Analogously, we can derive similar expressions for SARSA:

$$\mathcal{E}_{\text{TD}}^\theta(t) = r^{(t+1)} - \gamma F^\theta(\mathbf{s}^{(t+1)}, \mathbf{a}^{(t+1)}) + F^\theta(\mathbf{s}^{(t)}, \mathbf{a}^{(t)})$$

and PS:

$$\mathcal{E}_{\text{PS}}^\theta(t) = r^{(t+1)} + \gamma_{\text{ps}} F^\theta(\mathbf{s}^{(t)}, \mathbf{a}^{(t)})$$

It is then straightforward to derive an update rule for the weights of the RBM ($\theta^{(t+1)} = \theta^{(t)} + \Delta\theta$) by performing gradient descent on the squared error $\mathcal{E}^\theta(t)$ ²:

$$\begin{aligned} \Delta\theta &= -\frac{\alpha}{2} \nabla_{\theta} (\mathcal{E}^\theta(t))^2 \\ &= -\alpha \mathcal{E}^\theta(t) \nabla_{\theta} \mathcal{E}^\theta(t) \\ &\approx^4 -\alpha \mathcal{E}^\theta(t) \nabla_{\theta} F^\theta(\mathbf{s}^{(t)}, \mathbf{a}^{(t)}) \end{aligned} \quad (9)$$

It turns out that, in the case of RBMs, these values can be computed efficiently since the gradient of their free energy $\nabla_{\theta} F^\theta(\mathbf{v})$ has a tractable expression:

$$\begin{cases} \frac{\partial F^\theta(\mathbf{v})}{\partial w_{ik}} = -v_i \langle h_k \rangle_{P(\mathbf{h}|\mathbf{v})} \\ \frac{\partial F^\theta(\mathbf{v})}{\partial b_i} = -v_i ; \frac{\partial F^\theta(\mathbf{v})}{\partial b_k} = -\langle h_k \rangle_{P(\mathbf{h}|\mathbf{v})} \end{cases}$$

where $\langle h_k \rangle_{P(\mathbf{h}|\mathbf{v})} = 1 / (1 + \exp(-\sum_i w_{ik} v_i - b_k))$

B. From shallow to deep

Universal function approximation. The RBM-based model presented above fulfills one of our requirements: having a parameterized representation of the merit function that allows us to generalize learned behavior to unobserved states and actions. A natural consideration that arises from this approximation method is a possible compromise in representational power: a tabular method can represent arbitrary real-valued functions over the

³Under maximum likelihood learning. In practice, a different gradient is used to train RBMs, derived by the *contrastive divergence* method [55, 56]. Even though this gradient is computed more efficiently, it can lead to very large approximation errors in the learned distributions [57]

⁴The approximation comes in SARSA/ Q -learning from considering $Q(\mathbf{s}^{(t+1)}, \mathbf{a})$ constant with respect to θ , which is an assumption made in temporal difference learning.

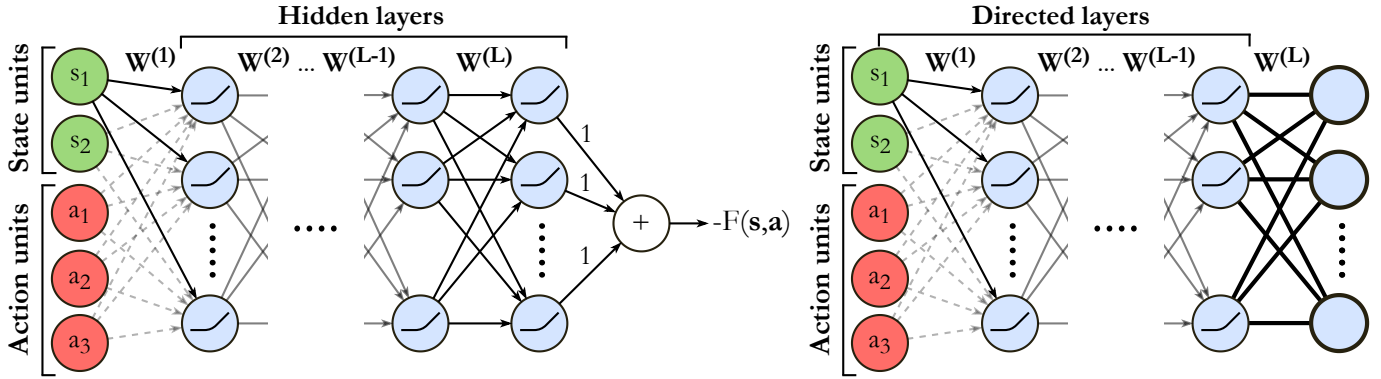


Figure 6. **The DEBN we consider and its corresponding DEM.** The DEM is obtained by removing the summation unit at the output of its corresponding DEBN and by replacing its last hidden layer with a layer of stochastic units of the same size. Just as in an RBM, these stochastic units can take binary values depending on the input given by their undirected connections. Biases are not represented for compactness.

state-action space, but there is no guarantee, a priori, that the RBM free energy can represent these functions with finitely many hidden units. Fortunately, a result from Le Roux & Bengio [58] shows that RBMs are universal function approximators: an RBM can represent arbitrary probability distributions over its visible units with any given precision, using a finite number of hidden units that depends on this distribution and the desired precision. This same result can be extended to prove that RBMs can represent arbitrary conditional probability distributions (i.e., policies) [59]. Unfortunately, these universality results also suggest that certain policies may need a number of hidden units that is linear in the number of state-action pairs to be represented precisely [60]⁵. This leads to a neural network parameterized by a *very large* number of weights, rendering it difficult to train and likely to overfit on a certain suboptimal behavior for general environments.

Deep energy-based network (DEBN). In contrast, deep neural networks are strictly more expressive: the Vapnik–Chervonenkis dimension [61], which is a measure of the expressive power of function approximators, of ReLU networks (the ones under consideration) grows linearly with their number of hidden layers when keeping their number of weights fixed [62]. Intuitively, this is the reason why deep neural networks require exponentially fewer weights than their shallow counterparts to represent a certain general class of functions [63]. Given the greater representational power of deep neural networks, we come back to the connection between the RBM-based approach and feedforward neural networks made in the previous section and extend the free energy network in Fig. 5 to a deep architecture by duplicating

its hidden layer. The resulting neural network represents the free energy (i.e., the energy after tracing out the *stochastic* hidden units) of a so-called deep energy model (DEM) (see Fig. 6), first introduced by Ngiam et al. [52]. As pointed out by the authors, this model is different from both deep Boltzmann machines (DBMs) [64] and deep belief networks (DBNs) [65] due to its *directed deterministic* connections between its first layers, followed by a *single* undirected stochastic layer. Conceptually, this model transforms state-action pairs given as input into non-linear features that are then treated as the visible units of an RBM. This construction preserves the tractability of the free energy inherited from the RBM (as opposed to DBMs and DBNs) while representing high-level abstractions of state-action pairs. Hence, the DEBNs fulfill our second requirement of having a model with large representational power without the associated drawback of having a large number of weights to train.

Updating the merit function. As for the RBM, updates of the merit function are performed through gradient descent on the weights of the DEBN. However, due to the deep architecture of the neural network, we have to resort to *backpropagation* [66] to propagate derivatives of the temporal difference error through the multiple layers of the DEBN. It can be easily verified that backpropagation of the temporal difference error on the shallow DEBN considered in the previous subsection leads to the same update rule as in Eq. (9).

Stable learning. Prior to the DQN of Mnih et al. [7], it was widely believed that non-linear function approximation using (deep) neural networks was not suited to learning value functions due to its high instability, which is likely to lead to divergence from the optimal value function [6]. This instability originates from the approximation of the target value function (see Eq. (8)) that leads to a non-stationary temporal difference error and from the high dependence between the training samples generated by the agent, both violating the assumptions behind con-

⁵Representing arbitrary merit functions using an RBM free-energy network (Fig. 5) has a similar cost in the number of hidden units [51].

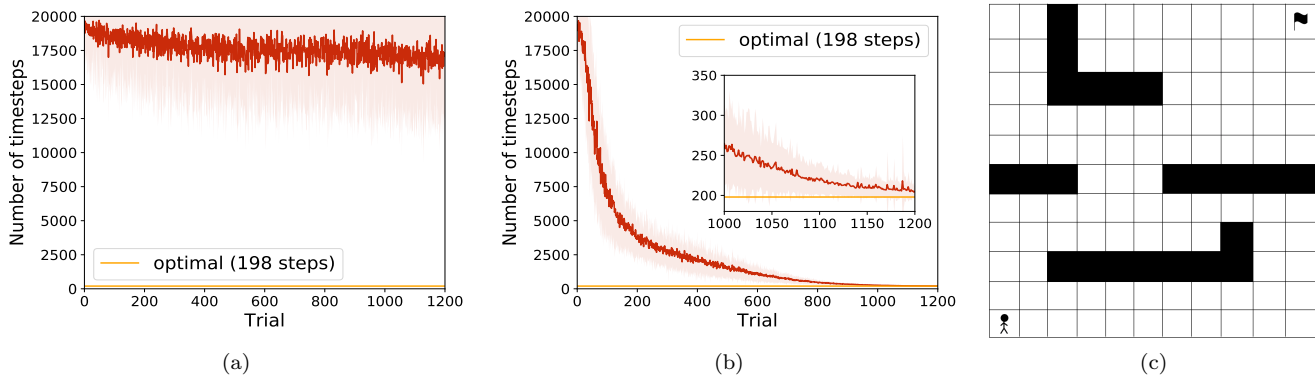


Figure 7. **Numerical comparison of tabular methods and shallow energy-based networks for a 100×100 GridWorld task.** (a) and (b) In both plots, the optimal performance (198 timesteps) is indicated by the orange curve. The red curves indicate the average performance and standard deviations of 50 agents. (a) The performance of tabular agents remains close to that of a random walk on the grid. (b) Agents with a shallow neural network reach close to optimal performance in their last 200 trials. (c) An illustrative depiction of the GridWorld environment. Note that this image is purely illustrative as it does not reflect the actual size and layout of the grid used in the simulations.

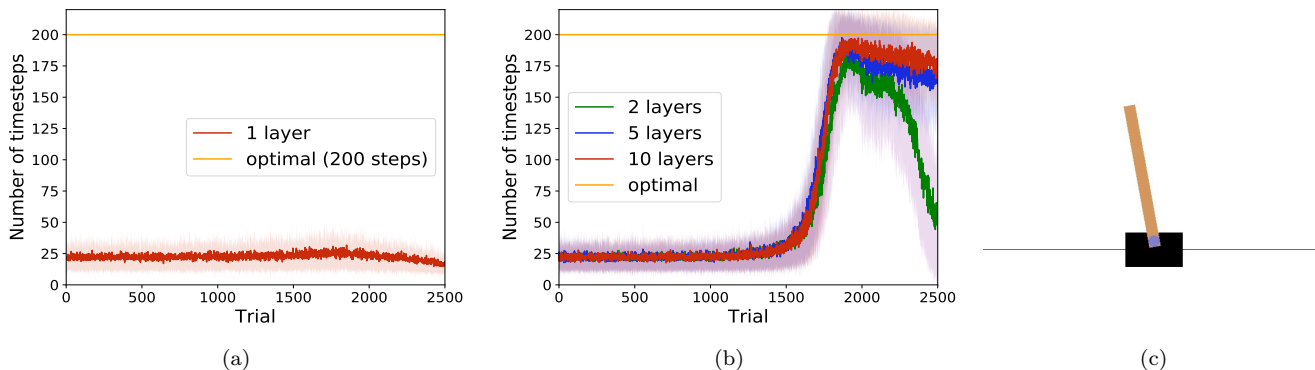


Figure 8. **Numerical comparison of shallow and deep energy-based networks in the Cartpole-v0 environment.** (a) and (b) In both plots, the optimal performance (200 timesteps) is indicated by the orange curve. The remaining curves indicate the average performance and standard deviations of 50 agents. (a) Agents with a shallow neural network exhibit close to random behavior. (b) We compare the average performance of neural networks with two, five and ten hidden layers and observe that the stability of the learned policy increases with the number of layers. (c) A game-screen image of the Cartpole-v0 environment.

vergence proofs in (un)supervised learning. Mainly two additions enabled stable learning with DQNs: 1. an *experience replay memory* storing (recent) samples of learning experience, used to generate decorrelated training data for the neural network; 2. a *target network*, i.e., a copy of the trained DQN updated at a slower rate, used to supply consistent targets for the temporal difference error during updates of the primary DQN. Naturally, we also rely on these tools to stabilize learning with our DEBNs.

C. Numerical simulations

In this subsection, we provide numerical evidence to the claims made above. First, we numerically compare the performance of tabular methods and shallow energy-based neural networks in a benchmarking task with a large and discrete state space. Then, we numerically

show the limitations of shallow architectures as opposed to deep ones in a benchmarking task with a continuous state space. The results are presented in Figs. 7 and 8.

GridWorld simulations. In order to demonstrate the advantage of shallow energy-based networks over tabular methods, we compare their performance in the GridWorld benchmarking task [67] (see Fig. 7c). In this task, the agent navigates through a two-dimensional array of cells by choosing, at each timestep of interaction, one of the four main cardinal directions to move from one cell to the next. The training is divided into trials. At the beginning of each trial, the position of the agent is initialized at a fixed starting cell $(0, 0)$ and a reward is placed in a fixed goal cell (n, n) , where n is the grid size. A trial terminates if the agent reaches the goal cell or if the length of the trial exceeds 20 000 timesteps. In the former case, the agent receives a reward of 1. In

the latter, the agent receives a reward of -1 . For the simulations presented here, we chose a 100×100 -grid with closed boundary conditions and no obstacles such that the state space is made large while maintaining a simple optimal policy, close to being state-independent (going up or right with equiprobability, except at the boundaries). In Fig. 7, we numerically demonstrate that agents using a shallow neural network architecture largely outperform their tabular counterparts in this task. This improved performance is expected due to the generalization capabilities provided by the neural network. The tabular methods are unable to detect and exploit the similarities between different cells.

Cartpole simulations. We now show, by means of an example, that DEBNs may provide advantages over shallow architectures in task environments with complex state spaces. More specifically, we consider the OpenAI Gym Cartpole-v0 environment [68] which features a continuous state space. In Cartpole, the goal is to balance in its unstable equilibrium an inverted pole-pendulum mounted on a movable cart by applying, at each timestep of interaction, a unit of force to the left or right (see Fig. 8c). A trial terminates if the angle between the vertical line above the pivot point and the pole exceeds 12° , if the center of mass of the cart is at a horizontal position outside the range $[-2.4, 2.4]$, or if the pendulum was successfully balanced for 200 consecutive timesteps. For every timestep the agent manages to balance the pole, it receives a reward of 1. The state space of this task can be described by four continuous parameters: the position of the cart, the velocity of the cart, the angle between the vertical line above the pivot point and the pole, and the angular velocity of the pole. In Fig. 8, we compare the performance of architectures with one, two, five and ten hidden layers. We observe that a single hidden layer is not sufficient to learn the complex optimal policy of this task. Given a DEBN with two hidden layers, a significant improvement of the learned policy can be observed. However, the performance of agents with five or ten hidden layers is more stable and closer to optimal behavior, due to their increased representational power.

Remarks. These classical simulations of benchmarking tasks demonstrate the advantages of a deep energy-based architecture for the PS update rule of the merit function. We can however argue that value-based methods exhibit similar behavior. This claim is supported by an extensive numerical study that showed the comparable performance of two-layered PS and tabular VBMs for similar benchmarking tasks [67]. Given the small size of the action space in both of the tasks considered here, we used *exact* sampling (see Sec. IV) from the policy of the agents. Results that showcase the advantages of the DEBN in tasks with large action spaces are left for future versions of this paper. The quantum speed-up presented in this paper applies to problems with large action spaces and

hence can not be numerically demonstrated as classical simulations are intractable.

IV. RANDOM-WALK DELIBERATION AND QUANTUM SPEED-UP

In the previous section, we showed how the approach of Sallans & Hinton that relies on energy-based models can be related to the deep RL framework of Mnih et al., a connection that led to the DEBNs we propose in this paper. But these, similarly to the RBMs considered in this earlier work, suffer from a serious caveat: sampling, even approximately, from their associated policies (i.e., deliberating on an action) is an NP-hard problem [53] for large action spaces. It is easy to see that *exact* sampling is intractable, since it requires computing the merit values $M^\theta(\mathbf{s}, \mathbf{a})$ of all possible actions \mathbf{a} given a state \mathbf{s} , which costs $\mathcal{O}(|\mathcal{A}|)$ evaluations of the DEBN. In practice, *approximate* sampling methods based on Markov chain Monte Carlo (MCMC), that is to say random walk processes, are preferred. While these methods may be faster under certain circumstances, they can still be inefficient in general [57, 69]. This makes quantum speed-ups particularly valuable.

In this section, we draw a connection between approximate sampling from DEBN policies to the random walk deliberation in PS in order to obtain a quantum speed-up in deliberation. To this end, we introduce Metropolis-Hastings and Gibbs sampling and describe how they generate Markov chains that have the desirable property of being reversible. Reversible Markov chains are at the core of the quantum speed-up in projective simulation, and we can use a similar approach to prove a speed-up in deliberation for DEBN agents.

A. Random-walk deliberation

Random walk on an ECM. In PS, sampling from the policy $\pi(\mathbf{a}|\mathbf{s})$ of an agent is done by a random walk on a weighted graph called the episodic and compositional memory (ECM). This deliberation process can be described as mixing a Markov chain (MC) $P_{\mathbf{s}}$ that acts on the nodes (or clips) of the ECM, and whose transition probabilities derive from the h -values weighting the edges between them. A trivial way to draw this MC is by preserving the connections of the ECM and by normalizing the outgoing h -values of all its clips. Generally though, this derivation leads to a non-reversible MC, rendering existing quantum walk algorithms inapplicable. In the case of a *two-layered* PS agents, Paparo et al. [26] showed that there exists an equivalent MC $P'_{\mathbf{s}}$ that acts exclusively on action clips and has the specificity of being *reversible*.

Similarly, in the case of our energy-based agents, we have

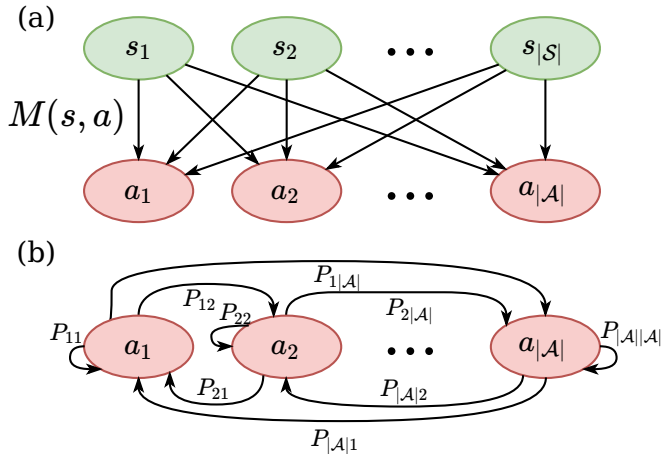


Figure 9. **Two ECMs derived for DEBN agents.** Note that the ECM (b) is state-specific, meaning that the complete ECM is made of $|\mathcal{S}|$ such ECMs.

the option to construct two ECMs to sample from their policies (see Fig. 9):

- **Two-layered ECM for exact sampling:** this ECM can be obtained by evaluating the merit values of all state-action pairs. Sampling consists in evaluating and normalizing the merit values of all actions given a state, leading to a $\mathcal{O}(|\mathcal{A}|)$ sampling complexity.
- **Monte Carlo ECM for approximate sampling:** this ECM is a reversible action-clip MC obtained from a MCMC algorithm such as Metropolis-Hastings [70] or Gibbs sampling [71], described below. Sampling consists in running a random walk on the ECM that starts in a random action-clip and is governed by the transition probabilities of the MC. It has a classical sampling complexity in $\tilde{\mathcal{O}}(\delta^{-1})$, where δ is the spectral gap of the MC.

Metropolis-Hastings (MH). The MH algorithm is a general MCMC method that allows one to sample from a probability distribution over a configuration space \mathcal{A} given only access to its corresponding density function, in our case $M^\theta(\mathbf{s}, \mathbf{a})$, without having to evaluate its value for all \mathbf{a} . To do so, MH constructs a reversible MC P having the desired distribution as stationary distribution by transforming a candidate transition matrix K into P . This construction starts by introducing an acceptance ratio $R_{\mathbf{a}\mathbf{a}'} = \min \left\{ 1, \frac{\exp(\beta M^\theta(\mathbf{s}, \mathbf{a}')) K_{\mathbf{a}'\mathbf{a}}}{\exp(\beta M^\theta(\mathbf{s}, \mathbf{a})) K_{\mathbf{a}\mathbf{a}'}} \right\}$ for each pair $(\mathbf{a}, \mathbf{a}') \in \mathcal{A}$ which is used to define P as follows:

$$P_{\mathbf{a}\mathbf{a}'} = \begin{cases} R_{\mathbf{a}\mathbf{a}'} K_{\mathbf{a}\mathbf{a}'} & \text{if } \mathbf{a}' \neq \mathbf{a} \\ 1 - \sum_{\mathbf{a}'' \neq \mathbf{a}} R_{\mathbf{a}\mathbf{a}''} K_{\mathbf{a}\mathbf{a}''} & \text{if } \mathbf{a}' = \mathbf{a} \end{cases} \quad (10)$$

In practice, K is chosen such that the sets $N(\mathbf{a}) = \{\mathbf{a}' : K_{\mathbf{a}\mathbf{a}'} > 0\}$ define a neighborhood structure on \mathcal{A} and $\max_{\mathbf{a} \in \mathcal{A}} |N(\mathbf{a})| \ll |\mathcal{A}|$. A possible choice for $N(\mathbf{a})$ and $K(\mathbf{a}, \cdot)$ is, e.g., a Hamming ball around \mathbf{a} and the uniform

distribution over it, respectively.

If $K_{\mathbf{a}\mathbf{a}'} > 0 \quad \forall \mathbf{a} \in \mathcal{A}$ and the graph defined by N is connected, then MH [70] ensures that P is reversible and has as stationary distribution:

$$\pi_\beta(\mathbf{a}|\mathbf{s}) = \frac{e^{\beta M^\theta(\mathbf{s}, \mathbf{a})}}{\sum_{\mathbf{a}'} e^{\beta M^\theta(\mathbf{s}, \mathbf{a}')}} \quad (11)$$

Gibbs sampling (GS). Gibbs sampling [71] is a particular instance of the Metropolis-Hastings algorithm where the neighborhood $N(\mathbf{a})$ is a Hamming ball of radius 1 around \mathbf{a} (including \mathbf{a} itself) and the candidate transition matrix K is given by:

$$K_{\mathbf{a}\mathbf{a}'} = \begin{cases} \frac{1}{\log |\mathcal{A}|} \frac{e^{\beta M^\theta(\mathbf{s}, \mathbf{a}')}}{e^{\beta M^\theta(\mathbf{s}, \mathbf{a})} + e^{\beta M^\theta(\mathbf{s}, \mathbf{a}')}} & \text{if } \mathbf{a}' \in N(\mathbf{a}) \\ 0 & \text{if } \mathbf{a}' \notin N(\mathbf{a}) \end{cases} \quad (12)$$

This K has the special property that its corresponding acceptance ratio $R_{\mathbf{a}\mathbf{a}'} = 1$ for all $\mathbf{a}' \in N(\mathbf{a})$. In particular, the conditions for reversibility of P are always met.

Runtime. Because MH and GS are random walk algorithms specified by reversible MCs, their runtime complexity depends on the spectral gap δ of their respective MCs. More precisely, this runtime, also called mixing time of the MC, is in $\tilde{\mathcal{O}}(\delta^{-1})$ [72]. A more detailed explanation is provided in Appendix B.

It is important to note that, while these random walk algorithms are much faster than exact sampling from their associated stationary distributions in certain use cases, they can be of comparable complexity in general. Indeed, in the case of RBM policies, it was shown that the mixing time of GS can be linear in the size of the action space $|\mathcal{A}|$ [57, 69]. More generally, approximating the partition function Z^θ of an arbitrary RBM is an NP-hard problem [53]. As a consequence of this result, there is a strong theoretical limit on what we can expect from approximate sampling algorithms.

Although it is conjectured (and supported by experimental evidence on different models) that deep representations lead to better mixing times [73], the previous theoretical argument can also be extended to DEBN policies: their corresponding energy model, the DEM, can be described as an RBM whose visible units are fed non-linear features of the DEBN's input. Hence, the theoretical limits of RBMs still apply to DEMs for general features.

B. Quantum deliberation

Due to the potentially high cost of sampling, quantum speed-ups for DEBN deliberation are of utmost importance. In the following, we give a brief description of the tools that can be used for a quantum deliberation and how they can be combined to achieve a quadratic speed-up over a classical random-walk deliberation.

Let P_β be the Markov chain issued by Metropolis-Hastings or Gibbs sampling and used to sample from

its stationary distribution π_β at inverse temperature β . Quantum deliberation consists in preparing the quantum state $|\pi_\beta\rangle = \sum_{\mathbf{a}} \sqrt{\pi_\beta(\mathbf{a}|\mathbf{s})} |\mathbf{a}\rangle$ and measuring it in the computational basis. We can prepare this state using a combination of fixed-point amplitude amplification (FPAA) [74, 75] and Szegedy quantum walks [27, 28]. As we explain below, *direct* preparation of $|\pi_\beta\rangle$ using these tools is intractable in general. That is why we additionally rely on an adaptive annealing schedule for the state preparation [76], described in this subsection.

Amplitude amplification. FPAA [75] allows one to transform an initial state $|\Psi\rangle$ into a target state $|\Psi'\rangle$ through a series of partial reflections $\Pi_\phi(\Psi)$ and $\Pi_\phi(\Psi')$ by an arbitrary angle ϕ around these states. This unitary transformation requires $\tilde{\mathcal{O}}(\sqrt{\gamma^{-1}})$ reflections, where γ is a lower bound on the overlap $|\langle\Psi|\Psi'\rangle|^2$.

Szegedy quantum walks. Szegedy walk operators [27, 28], in combination with the phase estimation algorithm [74], enable us to construct the reflections around $|\pi_\beta\rangle$ required for FPAA, as follows. Let P be a reversible Markov chain with stationary distribution π and spectral gap δ . Assuming $\mathcal{O}(1)$ coherent access to the columns of P , Refs. [27, 28] describe an efficient construction of the quantum walk operator $W(P)$. This $W(P)$ is a unitary whose unique⁶ eigenvalue-1 eigenvector is the coherent encoding $|\pi\rangle$ of π . It also has the valuable property that its phase gap Δ satisfies $\Delta \geq \sqrt{2\delta}$. Using the phase estimation algorithm [74], this allows us to construct an approximate reflector $\Pi_\phi(\pi)$ with $\tilde{\mathcal{O}}(\sqrt{\delta^{-1}})$ applications of $W(P)$. Note that, when the entries of P are computed by a classical circuit rather than being stored in memory, the cost of coherent access to the columns of P is the same as the cost of classical sampling from these columns [77]. This last point is explained in more detail in Appendix D.

Quantum simulated annealing. Direct preparation of $|\pi_\beta\rangle$ from an initial uniform superposition of all actions $|u\rangle = \sum_{\mathbf{a}} \sqrt{|\mathcal{A}|^{-1}} |\mathbf{a}\rangle$ using Szegedy walks and FPAA is intractable. Indeed, when π_β is a peaked distribution, the overlap $|\langle u|\pi_\beta\rangle|^2$ can be as small as $|\mathcal{A}|^{-1}$, leading to a total preparation complexity of $\tilde{\mathcal{O}}(\sqrt{\delta^{-1}}|\mathcal{A}|)$. To get around this issue, one can instead prepare several intermediary states $|u\rangle = |\pi_{\beta_0}\rangle, |\pi_{\beta_1}\rangle, \dots, |\pi_{\beta_l}\rangle$ following an *annealing schedule* on the inverse temperature β . More precisely, it was shown [78] that given a schedule $\beta_0 = 0, \beta_1, \dots, \beta_l = \beta$ and classical Markov chains $P_{\beta_0}, P_{\beta_1}, \dots, P_{\beta_l}$ with stationary distributions $\pi_{\beta_0}, \pi_{\beta_1}, \dots, \pi_{\beta_l}$ that fulfill the slow-varying condition $|\langle \pi_{\beta_i} | \pi_{\beta_{i+1}} \rangle|^2 \geq c$, preparing an ε -approximation of $|\pi_\beta\rangle$ has complexity $\mathcal{O}(\frac{l}{c} \sqrt{\delta^{-1}} \log^2(\frac{l}{\varepsilon}))$, where δ lower bounds the spectral gaps of these Markov chains.

Using an *adaptive* annealing schedule, Harrow & Wei [76] were able to provide a construction with length $l = \tilde{\mathcal{O}}(\sqrt{\log(Z(\beta)^{-1})}) \leq \tilde{\mathcal{O}}(\beta \|M^\theta\|)$ where $\|M^\theta\| = \max_{\mathbf{a}}(M^\theta(\mathbf{s}, \mathbf{a}))$, leading to a total preparation complexity of $\tilde{\mathcal{O}}(\sqrt{\delta^{-1}}\beta \|M^\theta\|)$.

Quantum DEBN agents. Given the classical description of a DEBN, i.e., a classical circuit that computes $M^\theta(\mathbf{s}, \mathbf{a})$ for a state-action pair as input, Metropolis-Hastings or Gibbs sampling give a classical description of the MC P_{β_i} which has the policy (11) as stationary distribution for arbitrary $\beta_i > 0$. Both of these can be used to create coherent access to the columns of P_{β_i} (see Appendix D) and hence use the Szegedy walk operators $W(P_{\beta_i})$ to perform quantum simulated annealing from the uniform superposition over all actions $|u\rangle$ to the desired state $|\pi_\beta\rangle$ in runtime $\tilde{\mathcal{O}}(\sqrt{\delta^{-1}}\beta \|M^\theta\|)$. Sampling then just requires measuring $|\pi_\beta\rangle$ in the computational basis. Thereby, we achieve a quadratic speed-up over the $\tilde{\mathcal{O}}(\delta^{-1})$ complexity of the classical random walk. Given the feedback from the environment following this quantum deliberation, the classical description of the DEBN is updated (according to the methods described in Sec. III B) and another round of deliberation starts.

V. RELATED WORK

QBM-RL. The work of Sallans & Hinton [30] using RBMs in a reinforcement learning context (see Sec. III A) has already been extended to the quantum domain by Crawford et al. [22, 50]. The authors first generalized the model to deep Boltzmann machines (DBMs), namely the concatenation of many RBMs in multiple layers, and then extended this approach to quantum Boltzmann machines (QBMs) [79]. Similarly to the classical BMs, QBMs are Ising spin models but with an additional transverse field acting on all the spins. This additional transverse field allows the application of quantum annealing [80], for instance, on a D-wave quantum annealer, to get an *empirical* advantage in sampling from the DBM policies. However, this approach does not have theoretical guarantees of speed-up compared to classical techniques and fails to sample from policies with effective low temperatures, i.e., $\beta \gg 0$. Moreover, the algorithmic approach presented in Refs. [22, 50] does not scale well with large action spaces and is incompatible with continuous state spaces. Note that, as explained by Ngiam et al. [52] and in Sec. III B, the approach presented in this paper is based on deep energy models (DEMs) which, as opposed to DBMs, have the particularity that their free energy can be expressed in the form of a feedforward neural network (the DEBN). This enables exact sampling in environments with small action spaces (which is intractable with DBMs) and allows us to introduce approximation only when the action space grows. In which case, the quantization helps to be quadratically faster.

⁶It is unique when restricted to the working subspace

Quantum algorithms for dynamic programming.

A recent paper [21] introduced quantum algorithms that solve Markov decision processes in a dynamic programming scenario. In this setting, the environment dynamics and reward function are known by the agent. Although these algorithms provide a quadratic speed-up over classical methods, they are, similarly to tabular methods, incompatible with environments having large state and action spaces as their runtime complexity scales with the square root of the size of the state-action space in the best case, i.e., $\Omega(\sqrt{|\mathcal{S}||\mathcal{A}|})$. The same argument as for tabular methods then applies: while neural networks do not overcome these lower bound complexities for general environments, they learn much faster in practice due to their generalization capabilities.

Deep energy-based RL. Similar deep energy-based neural networks have been used for RL in previous works. Haarnoja et al. [43] use the same type of neural networks in RL environments with continuous action spaces. Moreover, they rely on a second network for sampling [81], which is not guaranteed to sample from the actual policy encoded by the associated energy-based model. Dulac et al. [44], building upon the work of Lillicrap et al. [82], also use neural networks that are similar to DEBNs, but in an actor-critic scenario. In this work, an actor network produces a continuous “proto-action” and its k closest discrete actions are selected. These actions are compared by the critic using a DEBN-like network, and the one with the lowest free energy is executed on the environment. This scheme works better for higher values of k , but the complexity of sampling from the policy scales linearly with k . In principle, our approach for quantum approximate sampling can then be used to enhance this method when k is large.

Quantum PS. For clarification, note that, while the deliberation method presented in Sec. IV B and the one introduced by Paparo et al. [26] rely on the same tools, these differ in the type of random walks they rely on: the random walks used in that section are mixing-time random walks, as opposed to the hitting-time random walks used in their work. This difference is due to the additional structure on the ECMs the authors use (leading to *reflecting* PS agents) that constraints sampling from a subset of flagged actions only. More detailed explanations are deferred to Appendices A and B.

VI. CONCLUSION AND OUTLOOK

Recent years have seen a surge of interest in applying reinforcement learning to various technological and scientific problems. In this context, two methods are particularly noteworthy: so-called value-based methods [4] and projective simulation [25]. Both approaches have repeatedly proven their practicality in various task environments, ranging from robotics [83, 84] to science

[33, 35, 85]. In this work, we introduce a unifying framework for these two methods that relies on deep energy-based networks (DEBNs). DEBNs are capable of handling environments with complex state spaces and of encoding rich multimodal representations, which gives learning agents the capacity to generalize learned behavior over both state and action spaces. We provide numerical evidence in support of this thesis in two benchmarking tasks featuring both large discrete and continuous state spaces. Simulations that demonstrate the advantage of DEBNs in environments with large action spaces are left for a future version of this paper. Note, however, that generalization over actions comes at the cost of approximate sampling from a complex policy that may scale poorly with the number of possible actions. Therefore, we further prove a quantum advantage for the inference process of DEBNs using quantum walk algorithms. The quadratic speed-up resulting from this quantization is particularly valuable in the context of deep learning methods where already constant speed-ups offered by highly parallelized hardware (GPUs and TPUs) has played a major role in their success story. These results give a new perspective on the design of reinforcement learning agents in which quantum advantages allow to consider otherwise computationally prohibitive methods, paving the way to further improvements towards quantum reinforcement learning.

Note that the presented framework goes beyond the specific architecture or quantum algorithms used in this paper. As mentioned in the previous section, the framework itself is not limited to value-based methods but can also be extended to an actor-critic scenario [44], for which a quantum speed-up in deliberation can still be obtained. The framework is also not limited to the specific sampling methods used here. Instead, one could also use the quantum Gibbs sampler of van Apeldoorn & Gilyén [86], which is more advantageous than quantum walk algorithms in certain regimes. Finally, the quantum speed-up within our framework may not be limited to the deliberation, but one could further quantize the model itself by using, e.g., a quantum generative model [87] or a variational quantum circuit [88]. One would then gain an advantage from the representational power of these intrinsically quantum models without a compromise in the computation complexity of decision-making.

ACKNOWLEDGMENTS

SJ, HPN, LMT, and HJB acknowledge support from the Austrian Science Fund (FWF) through the projects DK-ALM:W1259-N27 and SFB BeyondC F71. SJ also acknowledges the Austrian Academy of Sciences as a recipient of the DOC Fellowship. HJB was also supported by the Ministerium für Wissenschaft, Forschung, und Kunst BadenWürttemberg (AZ:33-7533.-30-10/41/1). VD is funded through the Quantum Software Consortium.

-
- [1] I. Goodfellow, Y. Bengio, and A. Courville, *Deep Learning*. MIT Press, 2016. <http://www.deeplearningbook.org>.
- [2] A. Krizhevsky, I. Sutskever, and G. E. Hinton, “Imagenet classification with deep convolutional neural networks,” in *Advances in neural information processing systems*, pp. 1097–1105, 2012.
- [3] I. Goodfellow, J. Pouget-Abadie, M. Mirza, B. Xu, D. Warde-Farley, S. Ozair, A. Courville, and Y. Bengio, “Generative adversarial nets,” in *Advances in neural information processing systems*, pp. 2672–2680, 2014.
- [4] R. S. Sutton, A. G. Barto, *et al.*, *Reinforcement learning: An introduction*. 1998.
- [5] R. Bellman, R. Corporation, and K. M. R. Collection, *Dynamic Programming*. Rand Corporation research study, Princeton University Press, 1957.
- [6] J. N. Tsitsiklis and B. Van Roy, “Analysis of temporal-difference learning with function approximation,” in *Advances in neural information processing systems*, pp. 1075–1081, 1997.
- [7] V. Mnih, K. Kavukcuoglu, D. Silver, A. A. Rusu, J. Veness, M. G. Bellemare, A. Graves, M. Riedmiller, A. K. Fidjeland, G. Ostrovski, *et al.*, “Human-level control through deep reinforcement learning,” *Nature*, vol. 518, no. 7540, p. 529, 2015.
- [8] Y. Li, “Deep reinforcement learning: An overview,” *arXiv preprint arXiv:1701.07274*, 2017.
- [9] D. Silver, T. Hubert, J. Schrittwieser, I. Antonoglou, M. Lai, A. Guez, M. Lanctot, L. Sifre, D. Kumaran, T. Graepel, *et al.*, “A general reinforcement learning algorithm that masters chess, shogi, and go through self-play,” *Science*, vol. 362, no. 6419, pp. 1140–1144, 2018.
- [10] D. Silver, J. Schrittwieser, K. Simonyan, I. Antonoglou, A. Huang, A. Guez, T. Hubert, L. Baker, M. Lai, A. Bolton, *et al.*, “Mastering the game of go without human knowledge,” *Nature*, vol. 550, no. 7676, p. 354, 2017.
- [11] P. Mirowski, M. Grimes, M. Malinowski, K. M. Hermann, K. Anderson, D. Teplyashin, K. Simonyan, A. Zisserman, R. Hadsell, *et al.*, “Learning to navigate in cities without a map,” in *Advances in Neural Information Processing Systems*, pp. 2419–2430, 2018.
- [12] J. Biamonte, P. Wittek, N. Pancotti, P. Rebentrost, N. Wiebe, and S. Lloyd, “Quantum machine learning,” *Nature*, vol. 549, no. 7671, p. 195, 2017.
- [13] V. Dunjko and H. J. Briegel, “Machine learning & artificial intelligence in the quantum domain: a review of recent progress,” *Reports on Progress in Physics*, vol. 81, no. 7, p. 074001, 2018.
- [14] C. Ciliberto, M. Herbster, A. D. Ialongo, M. Pontil, A. Rocchetto, S. Severini, and L. Wossnig, “Quantum machine learning: a classical perspective,” *Proc. R. Soc. A*, vol. 474, no. 2209, p. 20170551, 2018.
- [15] M. Schuld, I. Sinayskiy, and F. Petruccione, “An introduction to quantum machine learning,” *Contemporary Physics*, vol. 56, no. 2, pp. 172–185, 2015.
- [16] J. Adcock, E. Allen, M. Day, S. Frick, J. Hinchliff, M. Johnson, S. Morley-Short, S. Pallister, A. Price, and S. Stanisic, “Advances in quantum machine learning,” *arXiv preprint arXiv:1512.02900*, 2015.
- [17] V. Dunjko, J. M. Taylor, and H. J. Briegel, “Advances in quantum reinforcement learning,” in *2017 IEEE International Conference on Systems, Man, and Cybernetics (SMC)*, pp. 282–287, IEEE, 2017.
- [18] V. Dunjko, Y.-K. Liu, X. Wu, and J. M. Taylor, “Exponential improvements for quantum-accessible reinforcement learning,” *arXiv preprint arXiv:1710.11160*, 2017.
- [19] V. Dunjko, J. M. Taylor, and H. J. Briegel, “Quantum-enhanced machine learning,” *Physical review letters*, vol. 117, no. 13, p. 130501, 2016.
- [20] V. Dunjko, J. M. Taylor, and H. J. Briegel, “Framework for learning agents in quantum environments,” *arXiv preprint arXiv:1507.08482*, 2015.
- [21] P. Ronagh, “Quantum algorithms for solving dynamic programming problems,” *arXiv preprint arXiv:1906.02229*, 2019.
- [22] A. Levit, D. Crawford, N. Ghadermarzy, J. S. Oberoi, E. Zahedinejad, and P. Ronagh, “Free energy-based reinforcement learning using a quantum processor,” *arXiv preprint arXiv:1706.00074*, 2017.
- [23] A. Cornelissen, “Quantum gradient estimation and its application to quantum reinforcement learning,” 2018.
- [24] F. Neukart, D. Von Dollen, C. Seidel, and G. Compostella, “Quantum-enhanced reinforcement learning for finite-episode games with discrete state spaces,” *Frontiers in Physics*, vol. 5, p. 71, 2018.
- [25] H. J. Briegel and G. De las Cuevas, “Projective simulation for artificial intelligence,” *Scientific reports*, vol. 2, p. 400, 2012.
- [26] G. D. Paparo, V. Dunjko, A. Makmal, M. A. Martin-Delgado, and H. J. Briegel, “Quantum speedup for active learning agents,” *Physical Review X*, vol. 4, no. 3, p. 031002, 2014.
- [27] M. Szegedy, “Quantum speed-up of markov chain based algorithms,” in *Foundations of Computer Science, 2004. Proceedings. 45th Annual IEEE Symposium on*, pp. 32–41, IEEE, 2004.
- [28] F. Magniez, A. Nayak, J. Roland, and M. Santha, “Search via quantum walk,” *SIAM Journal on Computing*, vol. 40, no. 1, pp. 142–164, 2011.
- [29] Y. Lecun, S. Chopra, R. Hadsell, M. A. Ranzato, and F. J. Huang, “A tutorial on energy-based learning,” in *Predicting structured data*, MIT Press, 2006.
- [30] B. Sallans and G. E. Hinton, “Reinforcement learning with factored states and actions,” *Journal of Machine Learning Research*, vol. 5, no. Aug, pp. 1063–1088, 2004.
- [31] M. August and J. M. Hernández-Lobato, “Taking gradients through experiments: Lstms and memory proximal policy optimization for black-box quantum control,” in *International Conference on High Performance Computing*, pp. 591–613, Springer, 2018.
- [32] T. Fösel, P. Tighineanu, T. Weiss, and F. Marquardt, “Reinforcement learning with neural networks for quantum feedback,” *Physical Review X*, vol. 8, no. 3, p. 031084, 2018.
- [33] M. Bukov, A. G. Day, D. Sels, P. Weinberg, A. Polkovnikov, and P. Mehta, “Reinforcement learning in different phases of quantum control,” *Physical Review X*, vol. 8, no. 3, p. 031086, 2018.
- [34] M. Bukov, “Reinforcement learning for autonomous preparation of floquet-engineered states: Inverting the

- quantum kapitza oscillator,” *Physical Review B*, vol. 98, no. 22, p. 224305, 2018.
- [35] H. P. Nautrup, N. Delfosse, V. Dunjko, H. J. Briegel, and N. Friis, “Optimizing quantum error correction codes with reinforcement learning,” *arXiv preprint arXiv:1812.08451*, 2018.
- [36] R. Sweke, M. S. Kesselring, E. P. van Nieuwenburg, and J. Eisert, “Reinforcement learning decoders for fault-tolerant quantum computation,” *arXiv preprint arXiv:1810.07207*, 2018.
- [37] P. Palittapongarnpim, P. Wittek, and B. C. Sanders, “Controlling adaptive quantum phase estimation with scalable reinforcement learning,” in *24th European Symposium on Artificial Neural Networks, Bruges, April 27–29, 2016*, pp. 327–332, 2016.
- [38] S. S. Vedaie, P. Palittapongarnpim, and B. C. Sanders, “Reinforcement learning for quantum metrology via quantum control,” in *2018 IEEE Photonics Society Summer Topical Meeting Series (SUM)*, pp. 163–164, IEEE, 2018.
- [39] R. Porotti, D. Tamascelli, M. Restelli, and E. Prati, “Coherent transport of quantum states by deep reinforcement learning,” *Communications Physics*, vol. 2, no. 1, p. 61, 2019.
- [40] J. Wallnöfer, A. A. Melnikov, W. Dür, and H. J. Briegel, “Machine learning for long-distance quantum communication,” *arXiv preprint arXiv:1904.10797*, 2019.
- [41] H. Xu, J. Li, L. Liu, Y. Wang, H. Yuan, and X. Wang, “Transferable control for quantum parameter estimation through reinforcement learning,” *arXiv preprint arXiv:1904.11298*, 2019.
- [42] M. Hessel, J. Modayil, H. Van Hasselt, T. Schaul, G. Ostrovski, W. Dabney, D. Horgan, B. Piot, M. Azar, and D. Silver, “Rainbow: Combining improvements in deep reinforcement learning,” in *Thirty-Second AAAI Conference on Artificial Intelligence*, 2018.
- [43] T. Haarnoja, H. Tang, P. Abbeel, and S. Levine, “Reinforcement learning with deep energy-based policies,” in *Proceedings of the 34th International Conference on Machine Learning—Volume 70*, pp. 1352–1361, JMLR. org, 2017.
- [44] G. Dulac-Arnold, R. Evans, H. van Hasselt, P. Sunehag, T. Lillicrap, J. Hunt, T. Mann, T. Weber, T. Degris, and B. Coppin, “Deep reinforcement learning in large discrete action spaces,” *arXiv preprint arXiv:1512.07679*, 2015.
- [45] G. E. Hinton and T. J. Sejnowski, “Optimal perceptual inference,” in *Proceedings of the IEEE conference on Computer Vision and Pattern Recognition*, pp. 448–453, Citeseer, 1983.
- [46] E. Ising, “Contribution to the theory of ferromagnetism,” *Z. Phys.*, vol. 31, pp. 253–258, 1925.
- [47] N. Heess, D. Silver, and Y. W. Teh, “Actor-critic reinforcement learning with energy-based policies,” in *Proceedings of the Tenth European Workshop on Reinforcement Learning*, vol. 24, pp. 45–58, PMLR, 2013.
- [48] M. Otsuka, J. Yoshimoto, and K. Doya, “Free-energy-based reinforcement learning in a partially observable environment,” in *ESANN*, 2010.
- [49] S. Elfving, E. Uchibe, and K. Doya, “From free energy to expected energy: Improving energy-based value function approximation in reinforcement learning,” *Neural Networks*, vol. 84, pp. 17–27, 2016.
- [50] D. Crawford, A. Levit, N. Ghadermarzy, J. S. Oberoi, and P. Ronagh, “Reinforcement learning using quantum boltzmann machines,” *arXiv preprint arXiv:1612.05695*, 2016.
- [51] J. Martens, A. Chattopadhyaya, T. Pitassi, and R. Zemel, “On the representational efficiency of restricted boltzmann machines,” in *Advances in Neural Information Processing Systems*, pp. 2877–2885, 2013.
- [52] J. Ngiam, Z. Chen, P. W. Koh, and A. Y. Ng, “Learning deep energy models,” in *Proceedings of the 28th international conference on machine learning (ICML-11)*, pp. 1105–1112, 2011.
- [53] P. M. Long and R. Servedio, “Restricted boltzmann machines are hard to approximately evaluate or simulate,” in *Proceedings of the 27th International Conference on Machine Learning (ICML-10)*, pp. 703–710, 2010.
- [54] G. E. Hinton, “A practical guide to training restricted boltzmann machines,” in *Neural networks: Tricks of the trade*, pp. 599–619, Springer, 2012.
- [55] M. Welling and G. E. Hinton, “A new learning algorithm for mean field boltzmann machines,” in *International Conference on Artificial Neural Networks*, pp. 351–357, Springer, 2002.
- [56] M. A. Carreira-Perpinan and G. E. Hinton, “On contrastive divergence learning,” in *Aistats*, vol. 10, pp. 33–40, Citeseer, 2005.
- [57] A. Fischer and C. Igel, “Bounding the bias of contrastive divergence learning,” *Neural computation*, vol. 23, no. 3, pp. 664–673, 2011.
- [58] N. Le Roux and Y. Bengio, “Representational power of restricted boltzmann machines and deep belief networks,” *Neural computation*, vol. 20, no. 6, pp. 1631–1649, 2008.
- [59] G. Montúfar, N. Ay, and K. Ghazi-Zahedi, “Geometry and expressive power of conditional restricted boltzmann machines,” *The Journal of Machine Learning Research*, vol. 16, no. 1, pp. 2405–2436, 2015.
- [60] G. F. Montúfar, J. Rauh, and N. Ay, “Expressive power and approximation errors of restricted boltzmann machines,” in *Advances in neural information processing systems*, pp. 415–423, 2011.
- [61] V. Vapnik and A. Y. Chervonenkis, “On the uniform convergence of relative frequencies of events to their probabilities,” *Measures of Complexity*, vol. 16, no. 2, p. 11, 1971.
- [62] N. Harvey, C. Liaw, and A. Mehrabian, “Nearly-tight vc-dimension bounds for piecewise linear neural networks,” in *Conference on Learning Theory*, pp. 1064–1068, 2017.
- [63] S. Liang and R. Srikant, “Why deep neural networks for function approximation?,” *arXiv preprint arXiv:1610.04161*, 2016.
- [64] R. Salakhutdinov and G. Hinton, “Deep boltzmann machines,” in *Artificial intelligence and statistics*, pp. 448–455, 2009.
- [65] G. E. Hinton, S. Osindero, and Y.-W. Teh, “A fast learning algorithm for deep belief nets,” *Neural computation*, vol. 18, no. 7, pp. 1527–1554, 2006.
- [66] D. E. Rumelhart, G. E. Hinton, R. J. Williams, *et al.*, “Learning representations by back-propagating errors,” *Cognitive modeling*, vol. 5, no. 3, p. 1.
- [67] A. A. Melnikov, A. Makmal, and H. J. Briegel, “Benchmarking projective simulation in navigation problems,” *IEEE Access*, vol. 6, pp. 64639–64648, 2018.
- [68] G. Brockman, V. Cheung, L. Petteysson, J. Schneider, J. Schulman, J. Tang, and W. Zaremba, “Openai gym,” *CoRR*, vol. abs/1606.01540, 2016.

- [69] P. Brémaud, *Markov chains: Gibbs fields, Monte Carlo simulation, and queues*, vol. 31. Springer Science & Business Media, 2013.
- [70] W. K. Hastings, “Monte carlo sampling methods using markov chains and their applications,” 1970.
- [71] S. Geman and D. Geman, “Stochastic relaxation, gibbs distributions, and the bayesian restoration of images,” *IEEE Transactions on pattern analysis and machine intelligence*, no. 6, pp. 721–741, 1984.
- [72] D. J. Aldous, “Some inequalities for reversible markov chains,” *Journal of the London Mathematical Society*, vol. 2, no. 3, pp. 564–576, 1982.
- [73] Y. Bengio, G. Mesnil, Y. Dauphin, and S. Rifai, “Better mixing via deep representations,” in *International conference on machine learning*, pp. 552–560, 2013.
- [74] G. Brassard, M. Mosca, and A. Tapp, “Quantum amplitude amplification and estimation,” *Contemporary Mathematics*, vol. 305, pp. 53–74, 2002.
- [75] T. J. Yoder, G. H. Low, and I. L. Chuang, “Fixed-point quantum search with an optimal number of queries,” *Physical review letters*, vol. 113, no. 21, p. 210501, 2014.
- [76] A. W. Harrow and A. Y. Wei, “Adaptive quantum simulated annealing for bayesian inference and estimating partition functions,” *arXiv preprint arXiv:1907.09965*, 2019.
- [77] L. Grover and T. Rudolph, “Creating superpositions that correspond to efficiently integrable probability distributions,” *arXiv preprint quant-ph/0208112*, 2002.
- [78] P. Wocjan and A. Abeyesinghe, “Speedup via quantum sampling,” *Physical Review A*, vol. 78, no. 4, p. 042336, 2008.
- [79] M. H. Amin, E. Andriyash, J. Rolfe, B. Kulchytskyy, and R. Melko, “Quantum boltzmann machine,” *Physical Review X*, vol. 8, no. 2, p. 021050, 2018.
- [80] S. W. Shin, G. Smith, J. A. Smolin, and U. Vazirani, “How” quantum” is the d-wave machine?,” *arXiv preprint arXiv:1401.7087*, 2014.
- [81] Q. Liu and D. Wang, “Stein variational gradient descent: A general purpose bayesian inference algorithm,” in *Advances in neural information processing systems*, pp. 2378–2386, 2016.
- [82] T. P. Lillicrap, J. J. Hunt, A. Pritzel, N. Heess, T. Erez, Y. Tassa, D. Silver, and D. Wierstra, “Continuous control with deep reinforcement learning,” *arXiv preprint arXiv:1509.02971*, 2015.
- [83] J. Kober, J. A. Bagnell, and J. Peters, “Reinforcement learning in robotics: A survey,” *The International Journal of Robotics Research*, vol. 32, no. 11, pp. 1238–1274, 2013.
- [84] S. Hangl, E. Ugur, S. Szedmak, and J. Piater, “Robotic playing for hierarchical complex skill learning,” in *2016 IEEE/RSJ International Conference on Intelligent Robots and Systems (IROS)*, pp. 2799–2804, IEEE, 2016.
- [85] A. A. Melnikov, H. P. Nautrup, M. Krenn, V. Dunjko, M. Tiersch, A. Zeilinger, and H. J. Briegel, “Active learning machine learns to create new quantum experiments,” *Proceedings of the National Academy of Sciences*, vol. 115, no. 6, pp. 1221–1226, 2018.
- [86] J. van Apeldoorn and A. Gilyén, “Improvements in quantum sdp-solving with applications,” *arXiv preprint arXiv:1804.05058*, 2018.
- [87] X. Gao, Z.-Y. Zhang, and L.-M. Duan, “A quantum machine learning algorithm based on generative models,” *Science advances*, vol. 4, no. 12, p. eaat9004, 2018.
- [88] S. Y.-C. Chen, C.-H. H. Yang, J. Qi, P.-Y. Chen, X. Ma, and H.-S. Goan, “Variational quantum circuits for deep reinforcement learning,” *arXiv preprint arXiv:1907.00397*, 2019.
- [89] D. H. Ackley, G. E. Hinton, and T. J. Sejnowski, “A learning algorithm for boltzmann machines,” *Cognitive science*, vol. 9, no. 1, pp. 147–169, 1985.
- [90] A. Fischer and C. Igel, “An introduction to restricted boltzmann machines,” in *Iberoamerican Congress on Pattern Recognition*, pp. 14–36, Springer, 2012.
- [91] M. A. Nielsen and I. L. Chuang, *Quantum Computation and Quantum Information*. Cambridge University Press, 2010.
- [92] V. Dunjko, N. Friis, and H. J. Briegel, “Quantum-enhanced deliberation of learning agents using trapped ions,” *New Journal of Physics*, vol. 17, no. 2, p. 023006, 2015.
- [93] D. P. Kingma and J. Ba, “Adam: A method for stochastic optimization,” *arXiv preprint arXiv:1412.6980*, 2014.

Appendix A: Introduction to reinforcement learning

A reinforcement learning scenario consists in a cyclic agent-environment interaction, where *states* (or, equivalently in the present context, *percepts*) \mathbf{s} , *actions* \mathbf{a} and *rewards* r are exchanged between the two parties. Every cycle of interaction is timed by a *timestep* t , such that a given interaction is described by a *history* $\mathbf{h} = (\mathbf{s}^{(0)}, \mathbf{a}^{(0)}, r^{(1)}, \mathbf{s}^{(1)}, \mathbf{a}^{(1)}, r^{(2)}, \dots)$.

Markov decision processes. We choose a common description of the environment in terms of a Markov decision process (MDP), defined by a set of *discrete* states \mathcal{S} , a set of *discrete* actions \mathcal{A} , a transition probability distribution $\mathcal{P} : \mathcal{S} \times \mathcal{A} \times \mathcal{S} \rightarrow \mathbb{R}_+$, a (stochastic) reward function $\mathcal{R} : \mathcal{S} \times \mathcal{A} \rightarrow \mathbb{R}$ and a discount factor of future rewards $\gamma \in [0, 1]$. Given that the state (action) space is discrete, we can assume that each state \mathbf{s} (action \mathbf{a}) is given a binary representation in $\{0, 1\}^{n_S}$ ($\{0, 1\}^{n_A}$), with $n_S = \lceil \log |\mathcal{S}| \rceil$ ($n_A = \lceil \log |\mathcal{A}| \rceil$). For every interaction history $\mathbf{h} = (\mathbf{s}^{(0)}, \mathbf{a}^{(0)}, r^{(1)}, \mathbf{s}^{(1)}, \mathbf{a}^{(1)}, r^{(2)}, \dots)$, we call *discounted return* the discounted sum of rewards⁷ $R = \sum_{t=1}^{\infty} \gamma^{t-1} r^{(t)}$, a figure of merit describing the performance of the agent on a given task. The goal of RL is to design agents that learn a policy $\pi : \mathcal{S} \times \mathcal{A} \rightarrow \mathbb{R}_+$ such that for any given state $\mathbf{s} \in \mathcal{S}$, the sampled action $\mathbf{a} \sim \pi(\mathbf{a}|\mathbf{s})$ maximizes the discounted return R for the remainder of the interaction. Even though this policy may not be unique, we call it the optimal policy π^* .

Value-based RL. So-called value-based methods in RL choose to resort to an additional function that explicitly links policy and return. The action-value function $Q(\mathbf{s}, \mathbf{a}) = \mathbb{E}_{\pi}[R | \mathbf{s}^{(0)} = \mathbf{s}, \mathbf{a}^{(0)} = \mathbf{a}]$, for instance, is the expected return given a state \mathbf{s} , in which the agent takes the action \mathbf{a} and follows a policy π thereafter. The Bellman equation [5] allows us to express Q recursively:

$$Q(\mathbf{s}, \mathbf{a}) = \mathcal{R}(\mathbf{s}, \mathbf{a}) + \gamma \sum_{\mathbf{s}', \mathbf{a}'} \mathcal{P}(\mathbf{s}' | \mathbf{s}, \mathbf{a}) \pi(\mathbf{a}' | \mathbf{s}') Q(\mathbf{s}', \mathbf{a}') \quad (\text{A1})$$

This recursive definition allows us to estimate the Q -function (that is, store *approximate* values $\hat{Q}(\mathbf{s}, \mathbf{a})$ of the action-value function for all *experienced* state-action pairs (\mathbf{s}, \mathbf{a})) from sample interactions with the environment while following a policy π . Through accumulated learning experience, the approximate values $\hat{Q}(\mathbf{s}, \mathbf{a})$ get closer and closer to those of the true Q -function for that policy.

In order to derive a policy from the stored \hat{Q} -values, a common transformation takes the form of a Boltzmann (or Gibbs) policy:

$$\pi(\mathbf{a}|\mathbf{s}) = \frac{e^{\beta \hat{Q}(\mathbf{s}, \mathbf{a})}}{\sum_{\mathbf{a}'} e^{\beta \hat{Q}(\mathbf{s}, \mathbf{a}')}} \quad (\text{A2})$$

where $\beta > 0$ is an inverse temperature parameter that allows us to adjust the degree of exploration (v.s. exploitation) of the policy.

It can be shown [4] that a general procedure which alternates between updating the stored values $\hat{Q}(\mathbf{s}, \mathbf{a})$ according to (one of several) update rule(s) derived from the Bellman equation and using these values to update the policy π of the agent according to Eq. (A2) leads to simultaneous convergence of \hat{Q} to the true Q -function and of π to the optimal policy π^* . Two common update rules, belonging to a larger family of *temporal difference (TD) learning* methods, are SARSA:

$$\hat{Q}(\mathbf{s}^{(t)}, \mathbf{a}^{(t)}) \leftarrow (1 - \alpha) \hat{Q}(\mathbf{s}^{(t)}, \mathbf{a}^{(t)}) + \alpha [r^{(t+1)} + \gamma \hat{Q}(\mathbf{s}^{(t+1)}, \mathbf{a}^{(t+1)})] \quad (\text{A3})$$

and Q -learning:

$$\hat{Q}(\mathbf{s}^{(t)}, \mathbf{a}^{(t)}) \leftarrow (1 - \alpha) \hat{Q}(\mathbf{s}^{(t)}, \mathbf{a}^{(t)}) + \alpha [r^{(t+1)} + \gamma \max_{\mathbf{a}} \hat{Q}(\mathbf{s}^{(t+1)}, \mathbf{a})] \quad (\text{A4})$$

where α is a learning rate in $[0, 1]$. It can be noticed that the target estimates for \hat{Q} -values in Q -learning differ from SARSA by that they are sampled from a 0-temperature (or greedy) policy $\pi(\mathbf{a}|\mathbf{s}) = \mathbb{1}_{\mathbf{a}} \left(\operatorname{argmax}_{\mathbf{a}'} \hat{Q}(\mathbf{s}, \mathbf{a}') \right)$.

Projective Simulation. Projective Simulation (PS) [25] is a physics-inspired approach for the design of autonomous learning agents which is different from the value-based methods presented above. The central component of a PS

⁷Note that for a discount factor $\gamma < 1$, this sum is ε -close to its first $\lceil \log_{\gamma} \frac{\varepsilon(1-\gamma)}{|R|_{\max}} \rceil$ terms, where $|R|_{\max} = \max_{\mathbf{s}, \mathbf{a}} \mathcal{R}(\mathbf{s}, \mathbf{a})$.

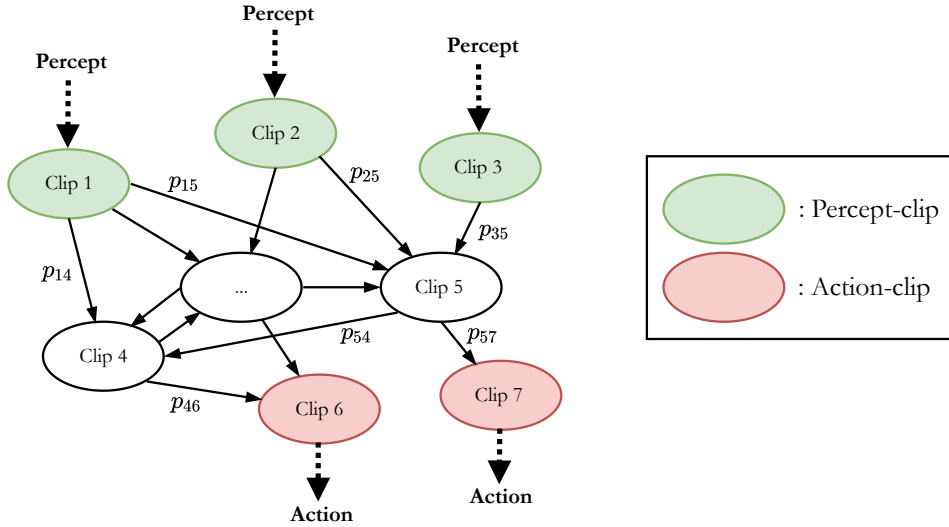


Figure 10. A generic Episodic and Compositional Memory

agent is its so-called Episodic and Compositional Memory (ECM), formally represented as a stochastic network of *clips* (see Fig. 10). Clips (the nodes of the stochastic network), represent short episodes, i.e., remembered sequences of percepts, rewards and actions, built upon experience of the agent through certain compositional methods applied on more basic clips: *percept-clips*, associated to single percepts perceived by the agent and *action-clips*, associated to single actions it can perform. In PS, the deliberation mechanism (that is, the selection of an action given a percept) is based on a random walk process, initiated at the percept-clip associated to the percept received at a certain time-step. There are several possibilities in which the random walk process can be realized, but in the basic PS, this consists in hopping between clips until an action-clip is hit. The action associated with that action-clip is then executed on the environment and its associated reward is used to update the weights (or transitions probabilities) of the ECM to increase the probability of the path that led to that action.

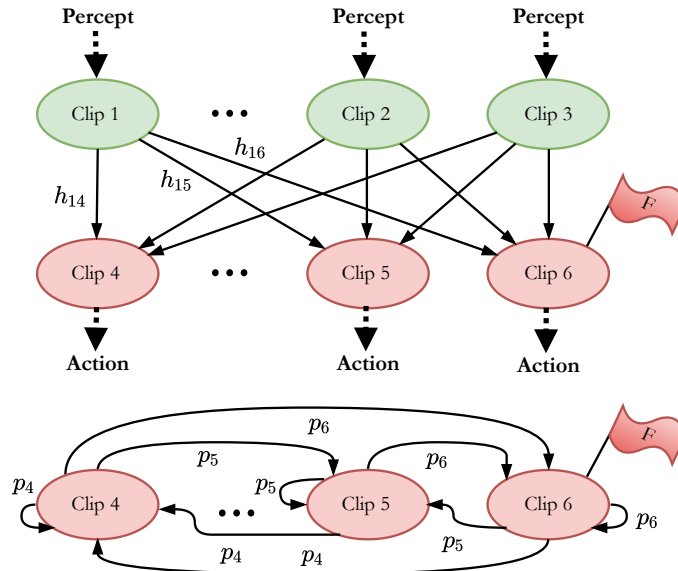


Figure 11. A two-layered ECM with flagged actions and its associated action-clip Markov chain

Two-layered PS. The simplest architecture of an ECM is given by the so-called *two-layered* PS (see Fig. 11): it is restricted to one layer of percept-clips linked to another layer of action-clips through weighted connections that we refer to as *h*-values. These are real-valued weights constrained to be greater than (and initialized at) 1. When

normalized according to, e.g., a Boltzmann distribution:

$$\pi(\mathbf{a} = j | \mathbf{s} = i) = \frac{e^{\beta h_{ij}}}{\sum_{j'} e^{\beta h_{ij'}}} \quad (\text{A5})$$

they give rise to the policy of the PS agent.

Learning takes place by updates of (all) h -values according to the following update rule:

$$h_{ij} \leftarrow h_{ij} - \gamma_{\text{ps}}(h_{ij} - 1) + g_{ij}\lambda \quad (\text{A6})$$

where $\gamma_{\text{ps}} \in [0, 1]$ is an internal damping (or forgetfulness) parameter allowing the agent to adapt to changing environments, λ is the last *positive* reward experienced by the agent, and the edge-glow g_{ij} is a varying rescaling factor accounting for delayed rewards.

Even though these h -values do not derive from the Bellman equation (Eq. (A1)) and hence cannot be described as a value function, we can see a clear connection between the policies in Eqs. (A2) and (A5): both methods rely on storing one real value per state-action pair and normalizing these values for each state/percept to derive a policy. Elaborating on this simple connection, it was shown that these methods have a comparable performance on benchmarking tasks [67].

Reflecting PS. The PS framework includes many additions to the basic architecture presented above. One of such additions consists in adding a short-term memory structure to the ECM network, in the form of flags assigned to the action clips. A flag indicates if the corresponding action, for a given percept, recently lead to a reward – a relevant information for agents in changing environments (not MDPs). The agent can use this additional information during his random walk on the ECM to deliberate on its next action: if the encountered action-clip isn't flagged, the random walk process can be reiterated, until a flagged action is hit or the process has been reiterated a maximum number of times R_{max} . This new deliberation process, called *reflecting*, can be equivalently described by a Markov chain (or random walk) on the space of action clips (see Fig. 11), where the transition probabilities are defined according to the last percept \mathbf{s}_i perceived by the agent. In the case of a two-layered PS agent, these transitions probabilities are:

$$p_j = \pi(\mathbf{a} = j | \mathbf{s} = i) = \frac{e^{\beta h_{ij}}}{\sum_{j'} e^{\beta h_{ij'}}} \quad (\text{A7})$$

The selection of a flagged action has then a time complexity governed by the *hitting time* of this Markov chain, which can benefit from a quadratic speed-up using quantum walks [26]. We define these notions in the next section.

Appendix B: Random and quantum walks

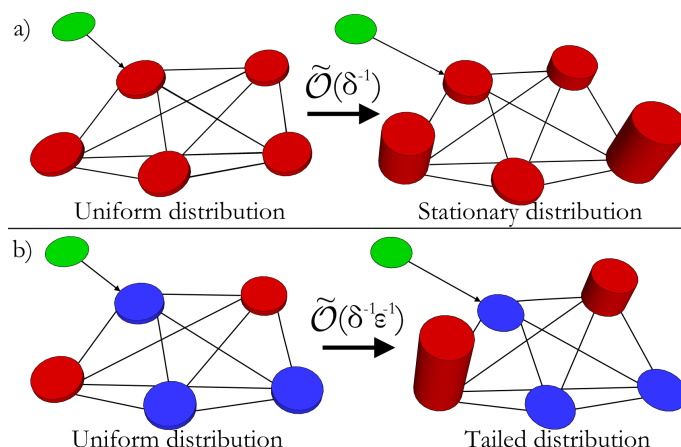


Figure 12. **Mixing-time v.s. Hitting-time random walks** Note that the graphs are generally non-symmetric (that is, the connections are directed), but were represented symmetric for simplicity. Marked elements are colored in red.

Mixing time. A discrete-time random walk on a graph is described by a Markov chain (MC) that is specified by a transition matrix P gathering the transition probabilities $[P]_{i,j} = P_{ij}$ from node i to node j of the graph. When the

MC is ergodic (i.e., irreducible and aperiodic), it has a unique stationary distribution $\boldsymbol{\pi} = P\boldsymbol{\pi}$ over the nodes of the graph. $\boldsymbol{\pi}$ can be approximated by repeated applications $P^t\boldsymbol{\pi}_0$ of P to any initial distribution $\boldsymbol{\pi}_0$, or equivalently, by applying t steps of the random walk P to any initial distribution $\boldsymbol{\pi}_0$ over the nodes of the graph. The minimal number of applications of P needed to obtain an ϵ' -close approximation of $\boldsymbol{\pi}$ (in l_p -norm) starting from *any* $\boldsymbol{\pi}_0$ is called the *mixing time* of P :

$$t_{\epsilon'}^{mix} = \min\{t : \forall \boldsymbol{\pi}_0, \|P^t\boldsymbol{\pi}_0 - \boldsymbol{\pi}\|_p \leq \epsilon'\} \quad (\text{B1})$$

When the MC is moreover reversible, its mixing time can be related to its spectral properties. More especially, we have [72]:

$$\left\lfloor \frac{1 - \delta}{2 \log(2\epsilon')} \frac{1}{\delta} \right\rfloor \leq t_{\epsilon'}^{mix} \leq \left\lceil \frac{1}{\delta} \log \left(\frac{1}{\epsilon' \pi^*} \right) \right\rceil \quad (\text{B2})$$

where $\delta = 1 - \max_{i>0} |\lambda_i| \in (0, 1]$ (i.e., the difference between the largest and second largest eigenvalues in absolute value of the matrix P) is the *spectral gap* of P and $\pi^* = \min_i \{\pi_i\}$. We say that the mixing time of a reversible MC P is of the order $\tilde{O}(\delta^{-1})$ ⁸.

Hitting time. Now suppose that the graph contains an (unknown) subset of marked nodes and that we are interested in finding one of these through a random walk on the graph. Let's call $\epsilon \in [0, 1]$ the proportion of marked elements in the stationary distribution $\boldsymbol{\pi}$ of P . Then note that a sample from $\boldsymbol{\pi}$ has probability ϵ of being marked, which implies that on average $1/\epsilon$ samples from $\boldsymbol{\pi}$ are needed to find a marked element. More generally, we are interested in preparing the *tailed distribution* of marked elements at stationarity $\boldsymbol{\pi}'$, which is the renormalized stationary distribution with support only on the marked nodes. The average number of random walk steps needed to prepare $\boldsymbol{\pi}'$ starting from any distribution $\boldsymbol{\pi}_0$ is called the *hitting time* of P and satisfies:

$$t_{\epsilon'}^{hit} = t_{\epsilon'}^{mix} / \epsilon \quad (\text{B3})$$

In the case of a reversible MC, the hitting time is of the order $\tilde{O}(\delta^{-1}\epsilon^{-1})$.

Szegedy walks. Szegedy-type quantum walks [27, 28] are a quantum analog of classical random walks. They generalize an MC P to a unitary $W(P)$ called the *Szegedy walk operator*. Here we describe how this unitary can be constructed and explain its interesting properties.

Let \mathcal{H} be the Hilbert space that shares the same basis vectors as the MC $P = [P_{ij}]$. So-called *quantum diffusion operators* U_P and V_P act on $\mathcal{H} \otimes \mathcal{H}$ as:

$$\begin{cases} U_P |i\rangle |0\rangle = |i\rangle \sum_j \sqrt{P_{ij}} |j\rangle \\ V_P |0\rangle |i\rangle = \sum_j \sqrt{P_{ij}^*} |j\rangle |i\rangle \end{cases}$$

where P^* is the time-reversed MC⁹ associated to P . Its elements are given by $P_{ij}^* = P_{ji}\pi_i/\pi_j$, where $\boldsymbol{\pi} = (\pi_i)$ is the stationary distribution of P . When $P^* = P$, we say that the MC is *reversible*. Although Szegedy walks can be defined if this property is not fulfilled, one would require additional access to P^* to be able to implement V_P . Because this is not usually the case (the expression of P^* involves the stationary distribution of P), the reversibility of P is then crucial for the implementation of V_P .

With the quantum diffusion operators U_P and V_P at hand, we can construct the Szegedy walk operator $W(P)$, which is the reflection over the spaces A and B :

$$\begin{cases} A = \text{span}\{U_P |i\rangle |0\rangle : i = 1, \dots, N\} \\ B = \text{span}\{V_P |0\rangle |i\rangle : i = 1, \dots, N\} \end{cases}$$

$$W(P) = \text{ref}(B) \text{ref}(A)$$

where

$$\begin{cases} \text{ref}(A) = U_P [\mathbb{1}_N \otimes \text{ref}(0)] U_P^\dagger \\ \text{ref}(B) = V_P [\text{ref}(0) \otimes \mathbb{1}_N] V_P^\dagger \end{cases}$$

⁸Intuitively, this has to do with the fact that all eigenvalues modulus of P are strictly less than 1 (except for the eigenvalue 1 associated to the stationary distribution), and repeated applications of P make its (non-eigenvalue-1) eigenspaces fade away with a geometric rate corresponding to their eigenvalue modulus. The slowest fading rate is given by the second largest eigenvalue modulus.

⁹Note that the asterisk on P^* does not indicate complex conjugation.

and

$$\text{ref}(0) = 2|0\rangle\langle 0| - \mathbb{1}_N$$

We refer to $A+B$ as the busy subspace and to its orthogonal complement $A^\perp \cap B^\perp$ as the idle subspace. $W(P)$ acts as the identity on the idle subspace, but, on the busy subspace, its unique eigenvector with eigenvalue 1 (or, equivalently, eigenphase 0) is

$$|\pi\rangle|0\rangle = \sum_i \sqrt{\pi_i} |i\rangle|0\rangle$$

This follows from Refs. [27, 28].

As we were interested in the spectral gap δ of P classically, we are interested in the *phase gap* $\Delta = 2 \min_{i>0} |\theta_i|$, i.e., the smallest non-zero eigenphase of $W(P)$, in the quantum case. Given that the eigenvalues of P and the eigenphases of $W(P)$ are related by $|\lambda_i| = \cos(\theta_i) \forall i$, it can be shown [27, 28] that:

$$\Delta \geq \sqrt{2\delta}$$

i.e., the phase gap of $W(P)$ is quadratically larger than the spectral gap of P . This is a crucial property for Szegedy quantum walks as a “quantum search” [74, 75] for $|\pi\rangle|0\rangle$ on the busy subspace of $W(P)$ is governed by its phase gap as $\tilde{\mathcal{O}}(\Delta^{-1})$. This is quadratically faster than sampling from π classically.

Note that, in the case of a two-layered reflecting PS agent, the quantum state $|\pi\rangle$ can be easily prepared, as the MC defined by the transition probabilities of Eq. (A7) has a trivial mixing time $\delta = 1$. This makes it a purely hitting-type random walk, for which one is interested in preparing $|\pi_F\rangle = \frac{1}{Z_F} \sum_{i \in F} \sqrt{\pi_i} |i\rangle$, where F is the set of flagged actions associated to a given percept. To this end, the authors of Ref. [26] use Szegedy walks and amplitude amplification [74, 75] to prepare $|\pi_F\rangle$ from $|\pi\rangle$. The complexity of this preparation is in $\tilde{\mathcal{O}}(\sqrt{\varepsilon^{-1}})$, where $\varepsilon = |\langle \pi | \pi_F \rangle|^2$. This is quadratically faster than the complexity of the classical random walk, in $\mathcal{O}(\varepsilon^{-1})$.

The quantum deliberation of Sec. IV B does not rely on flagged actions, and hence is a mixing-type random walk.

Appendix C: Boltzmann machines and energy-based models

Restricted Boltzmann machines. Boltzmann machines [89] are energy-based generative models, meaning that they can learn probability distributions $\hat{p}(\mathbf{x})$ over a set $\mathcal{X} \subset \{0, 1\}^n$, by encoding a parameterized distribution $p^\theta(\mathbf{x})$. This probability distribution is specified by an energy function $E^\theta(\mathbf{x})$ defined over the entire set \mathcal{X} and normalized by a Boltzmann/Gibbs distribution:

$$P^\theta(\mathbf{x}) = \frac{e^{-E^\theta(\mathbf{x})}}{\sum_{\mathbf{x}'} e^{-E^\theta(\mathbf{x}')}} \quad (\text{C1})$$

This energy function takes the form of an Ising model spin Hamiltonian which accounts for pair interactions w_{ik} and individual external magnetic fields b_i ($(\{w_{ik}\}_{i,k}, \{b_i\}_i) = \theta \in \mathbb{R}^d$) acting between and over spins x_i and x_k . Different configurations of these spins correspond to different binary vectors $\mathbf{x} \in \mathcal{X}$. A commonly used type of BMs are the so-called restricted Boltzmann machines [54, 90], characterized by their bipartite structure (see Fig. 4), which restricts the interactions w_{ik} in the Ising model Hamiltonian/energy function. RBMs divide the spins $\{x_i\}_i$ between two subsets $\mathbf{v} = \{v_i\}_i$ and $\mathbf{h} = \{h_k\}_k$, respectively called visible and hidden units. The visible units represent the data that we want to encode in the model, while the hidden (or latent) units allow to have more degrees of freedom in the specification of the energy function and allow to represent more complex distributions over the visible units. The RBM model effectively encodes the probability distribution:

$$P^\theta(\mathbf{v}) = \frac{\sum_{\mathbf{h}} e^{-E^\theta(\mathbf{v}, \mathbf{h})}}{\sum_{\mathbf{v}', \mathbf{h}'} e^{-E^\theta(\mathbf{v}', \mathbf{h}')}} = \frac{e^{-F^\theta(\mathbf{v})}}{\sum_{\mathbf{v}'} e^{-F^\theta(\mathbf{v}')}} \quad (\text{C2})$$

where

$$-E^\theta(\mathbf{v}, \mathbf{h}) = \sum_{i,k} w_{ik} v_i h_k + \sum_i b_i v_i + \sum_k b_k h_k \quad (\text{C3})$$

and

$$\begin{aligned}
F^\theta(\mathbf{v}) &= -\log \left(\sum_{\mathbf{h}'} e^{-E^\theta(\mathbf{v}, \mathbf{h}')} \right) \\
&= -\log \left(\frac{e^{-E^\theta(\mathbf{v}, \mathbf{h})}}{P(\mathbf{h}|\mathbf{v})} \right) \quad \forall \mathbf{h} \\
&= E^\theta(\mathbf{v}, \mathbf{h}) + \log(P(\mathbf{h}|\mathbf{v})) \quad \forall \mathbf{h} \\
&= \sum_{\mathbf{h}} P(\mathbf{h}|\mathbf{v}) [E^\theta(\mathbf{v}, \mathbf{h}) + \log(P(\mathbf{h}|\mathbf{v}))] \\
&= E^\theta(\mathbf{v}, \langle \mathbf{h} \rangle_{P(\mathbf{h}|\mathbf{v})}) + H(\mathbf{h}|\mathbf{v})
\end{aligned}$$

is the so-called *free energy* of the RBM (the average energy after tracing out the hidden units).

Derivation of the free-energy neural network. We derive below the expression of an RBM free energy as a feedforward neural network. This derivation is inspired by Ref. [51].

Starting from the expression of an RBM probability distribution:

$$\begin{aligned}
P^\theta(\mathbf{v}) &= \frac{1}{Z^\theta} \sum_{\mathbf{h}} \exp \left(\sum_{i,k} w_{ik} v_i h_k + \sum_i b_i v_i + \sum_k b_k h_k \right) \\
&= \frac{1}{Z^\theta} \exp \left(\sum_i b_i v_i \right) \prod_k \sum_{h_k \in \{0,1\}} \exp \left(\sum_i w_{ik} v_i h_k + b_k h_k \right) \# \sum_{\mathbf{x} \in \{0,1\}^2} e^{ax_1 + bx_2} = (1 + e^a)(1 + e^b) \\
&= \frac{1}{Z^\theta} \exp \left(\sum_i b_i v_i \right) \prod_k \left(1 + \exp \left(\sum_i w_{ik} v_i + b_k \right) \right) \# \sum_{\mathbf{x} \in \{0,1\}^2} e^{ax_1 + bx_2} = (1 + e^a)(1 + e^b) \\
&= \frac{1}{Z^\theta} \exp \left(\sum_i b_i v_i \right) \exp \left(\sum_k \log \left(1 + \exp \left(\sum_i w_{ik} v_i + b_k \right) \right) \right) \# \prod_k a_k = \exp \left(\sum_k \log(a_k) \right) \\
&= \frac{1}{Z^\theta} \exp \left(\sum_i b_i v_i + \sum_k \text{softplus} \left(\sum_i w_{ik} v_i + b_k \right) \right) \# \text{softplus}(x) = \log(1 + \exp(x)) \\
&= \frac{1}{Z^\theta} \exp(-F^\theta(\mathbf{v}))
\end{aligned}$$

we end up with:

$$-F^\theta(\mathbf{v}) = \sum_i b_i v_i + \sum_k \text{softplus} \left(\sum_i w_{ik} v_i + b_k \right) \quad (\text{C4})$$

which takes the form of the feedforward neural network depicted in Fig. 5.

Derivation of the PS error function. We showed in Sec. III A how to derive an error function from the Q -learning update rule. Due to its shared origin, deriving an error function from the SARSA update rule can be done similarly. In contrast, h -values are not linked to the Bellmann equation and hence do not represent estimates of the (bounded) return. Instead, they are allowed to accumulate rewards indefinitely (and hence diverge). Diverging h -values can still lead to converging policies after normalization but they constitute a problem for the derivation of an error function, as this error can never be minimized to 0, hence making neural networks harder to train. One mechanism in PS that allows us to avoid this divergence is damping, and we show here how it can be translated into a regularization term in the PS error function.

Let's take the update rule of PS (Eq. (A6)) with damping $\gamma_{\text{ps}} = 0$ and edge-glow $g_{ij} = 1$:

$$h_{ij} \leftarrow h_{ij} + \lambda \quad (\text{C5})$$

This setup cancels the damping mechanism and supposes that edge-glow values $g_{ij} \neq 1$ are absorbed in the reward λ . This update rule gives the following error function:

$$\mathcal{E}_{\text{PS}}(\mathbf{s}^{(t)}, \mathbf{a}^{(t)}) = r^{(t+1)} \quad (\text{C6})$$

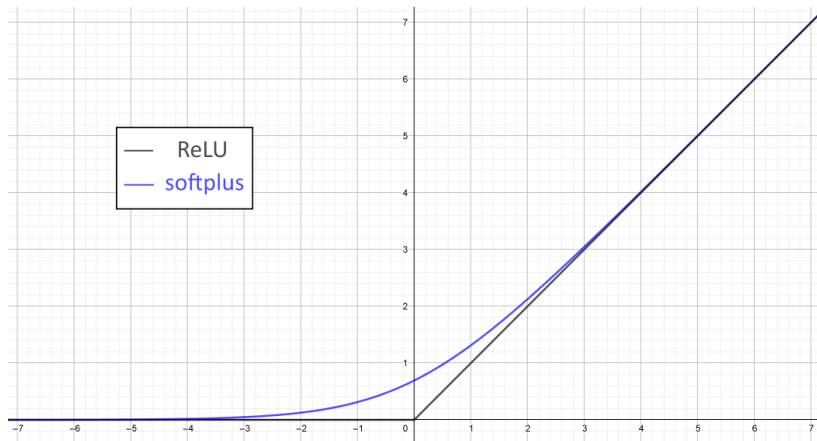


Figure 13. **A comparison between the commonly used ReLU activation function $\max(0, x)$ and the softplus function $x + \log(1 + e^{-x}) = \log(1 + e^x)$ appearing in the expression of the free energy of an RBM**

which is never 0 as long as the given transition is rewarded (which is the case in a static environment) and leads to diverging h -values.

To avoid this divergence, we take into account damping by effectively introducing a regularization term:

$$\mathcal{E}_{\text{PS}}(\mathbf{s}^{(t)}, \mathbf{a}^{(t)}) = r^{(t+1)} - \gamma_{\text{ps}} h_{ij} \quad (\text{C7})$$

such that the error is now 0 when $h_{ij} = r^{(t+1)}/\gamma_{\text{ps}}$, hence effectively bounding the h -values. Note that $\mathcal{E}_{\text{PS}}(\mathbf{s}^{(t)}, \mathbf{a}^{(t)}) = h_{ij}^{(t+1)} - h_{ij}^{(t)}$, so this new error corresponds to the update rule:

$$h_{ij} \leftarrow (1 - \gamma_{\text{ps}}) h_{ij} + \lambda \quad (\text{C8})$$

which is the original PS update rule (Eq. (A6), with the edge-glow fixed to 1).

Appendix D: Coherent access to the transition matrix

We want to implement the operation $|i\rangle_1 |0\rangle_2 |0\rangle_{aux} \rightarrow |i\rangle_1 \sum_{j \in N(i)} \sqrt{P_{ij}} |j\rangle_2 |0\rangle_{aux}$ coherently for all actions i and for the transition matrix P and neighborhood structure N given by Metropolis-Hastings or Gibbs sampling (Sec. IV A). In order to achieve this, we assume access to the description of the classical circuits that compute the operations $|i\rangle_1 |j\rangle_2 |0\rangle \rightarrow |i\rangle_1 |j\rangle_2 |P_{ij}\rangle$ and $|i\rangle |0\rangle \rightarrow |i\rangle \otimes_{j \in N(i)} |j\rangle$, having complexity $C(P)$ and $\mathcal{O}(\text{poly}(M))$ respectively. Using either Fredkin or Toffoli gates, it is possible to design quantum circuits that implement coherently the operation $|i\rangle |0\rangle^{\otimes M} |0\rangle_{aux} \rightarrow |i\rangle |P_{i1}\rangle \dots |P_{iM}\rangle |0\rangle_{aux}$ with comparable complexities by *reversibilization* (Sec. 3.2.5. of [91]), where $M = \max_{a \in \mathcal{A}} N(a)$ and the $j \in N(i)$ have been renamed $1, \dots, M$ for each i for simplicity. Using this circuit and a procedure called *coherent controlization* [77, 92], it is possible to implement the coherent access to the columns of the transition matrix P using $\mathcal{O}(M \times C(P) + \text{poly}(M))$ operations, same as classically. This implementation goes as follows:

$$\begin{aligned} & |i\rangle_1 |0\rangle_{aux}^{\otimes M} |0\rangle_{aux}^{\otimes M-2} |0\rangle_2^{\otimes \log(M)} \\ & \rightarrow |i\rangle_1 |P_{i1}\rangle \dots |P_{iM}\rangle |0\rangle_{aux}^{\otimes M-2} |0\rangle_2^{\otimes \log(M)} \quad \# \text{ cost } M \times C(P) + \mathcal{O}(\text{poly}(M)) \\ & \rightarrow |i\rangle_1 |P_{i1}\rangle \dots |P_{iM}\rangle \left| P_{i1} + \dots + P_{i\frac{M}{2}} \right\rangle \dots \left| P_{i, \frac{M}{2}-1} + P_{i\frac{M}{2}} \right\rangle |0\rangle_2^{\otimes \log(M)} \quad \# \text{ cost } M - 2 \text{ additions} \\ & \rightarrow |i\rangle_1 |P_{i1}\rangle \dots |P_{iM}\rangle \left| P_{i1} + \dots + P_{i\frac{M}{2}} \right\rangle \dots \left| P_{i, \frac{M}{2}-1} + P_{i\frac{M}{2}} \right\rangle \sum_{j=1}^M \sqrt{P_{ij}} |j\rangle_2 \quad \# \text{ cost of CC: } \mathcal{O}(\text{poly}(M)) \\ & \rightarrow |i\rangle_1 |0\rangle_{aux}^{\otimes M} |0\rangle_{aux}^{\otimes M-2} \sum_{j=1}^M \sqrt{P_{ij}} |j\rangle_2 \quad \# \text{ cost } M \times C(P) + \mathcal{O}(\text{poly}(M)) \end{aligned}$$

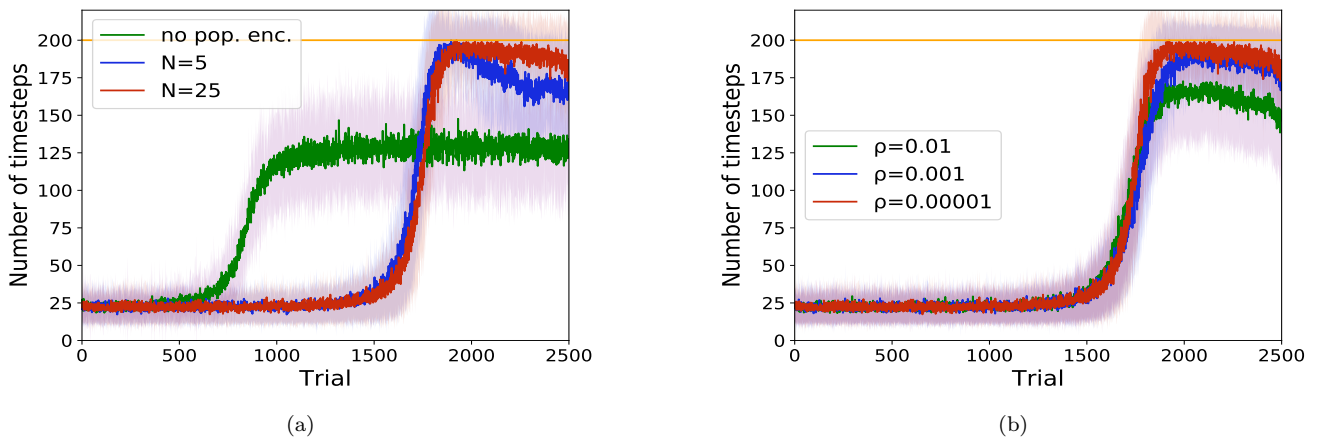


Figure 14. **Numerical investigation of the state encoding.** We encoded the states of the Cartpole-v0 environment using population encoding. For all curves, the average timesteps and the standard deviation of 50 agents are shown. The optimal performance (200 timesteps) is indicated by the orange line. (a) For the first simulation, we tested population encoding with 5 and 25 neurons. We additionally compare the resulting curves to the average learning curve of agents without population encoding. The highest number of neurons leads to a more stable optimal policy. (b) The second simulation shows how the average learning curve varies under changing the ratio ρ of the excitation range a to the number of neurons N , for a fixed $N = 25$. An encoding with the ratio $\rho = 0.000001$ achieves a higher average reward. All neural networks used in these simulations have 10 hidden layers.

Appendix E: Details on the numerical simulations

Hyperparameters. For the simulations of GridWorld, we chose ADAM [93] as an optimizer with a learning rate of $\alpha = 0.0001$. The training batches of the main network contain 100 samples and the replay memory has a capacity of 5000 interactions. The target network is updated every 30 trials while the experience replay memory is updated every 100 timesteps (in a First-In-First-Out manner). We chose an exponential annealing schedule for the glow parameters of the PS update rule that starts with a value of 0.9 and ends with a value of 0.99. The agent’s policy is a softmax policy and for the β -parameter we choose a hyperbolic tangent schedule that starts with a value of 0.001 and ends with a value of 1. All neural networks have 64 units per layer.

For the simulations of Cartpole, we chose ADAM as an optimizer with a learning rate of $\alpha = 0.0001$. The training batches of the main network contain 100 samples and the replay memory has a capacity of 5000 interactions. The target network is updated every 30 trials while the experience replay memory is updated every 10 timesteps (in a First In First Out manner). We chose an exponential annealing schedule for the glow parameters of the PS update rule that starts with a value of 0.5 and ends with a value of 0.99. The agent’s policy is a softmax policy and for the β -parameter we choose a hyperbolic tangent schedule that starts with a value of 0.001 and ends with a value of 1. In order to have a fair comparison of the performance of neural networks with different depths, we set their number of units per hidden layer such that all neural networks have approximately the same total number of weights and biases. More precisely, we set the number of units per layer to be 25, 34, 53 and 80 for neural networks with respectively 10, 5, 2 and 1 hidden layer(s), leading to a total number of weights and biases of 8300, 8262, 8480, 8560 respectively.

Environment description. The GridWorld environment can be described as an array of cells. For our simulations, we chose a 100×100 grid, where each state (cell) is described by its x - and y -coordinates (x, y) . Each trial starts in the state $(1, 1)$ and the state $(100, 100)$ is the agent’s goal state. A trial terminates if its length exceeds 20 000 timesteps or if the agent reaches the goal state. In the latter case, the agent receives a reward of 1. Otherwise, it receives a reward of -1 . At each timestep, the agent performs one of four actions: moving up, down, left or right. Any policy leading to a trial of length 198 timesteps is optimal. We ran our simulations for 1200 trials.

Cartpole is an OpenAI Gym environment. For the presented numerical simulations we used the version Cartpole-v0. In this game, a pole is mounted on a movable cart. Each state in the game is described by four coordinates: the position of the cart, the velocity of the cart, the angle between the vertical line above the pivot point and the pole, and the angular velocity of the pole. For the starting state, the four coordinates are assigned a uniform random value between ± 0.05 . A trial terminates if the angle between the vertical line above the pivot point and the pole exceeds 12° , if the center of mass of the cart is at a position outside the range $[-2.4, 2.4]$ or if the pole is balanced for 200 steps. For every timestep the game is not terminated, the agent receives a reward of one. Any pol-

icy that allows the agent to balance the pole for 200 steps is considered optimal. We ran the simulations for 2500 trials.

State preprocessing. Both environments are fully observable since the transition function that determines the evolution of the system under the actions of the agent fulfills the Markov condition. In the case of GridWorld, each state can be described by two discrete coordinates, each of which will be one-hot encoded, i.e., each coordinate value is assigned a vector with one non-zero value equal to 1. The resulting two-hot encoded state is then fed into the neural network. In Cartpole, on the other hand, each state is described by four continuous coordinates and can be described by a four-dimensional vector \mathbf{x} . The first coordinate is the position of the center of mass of the cart which takes values between $[-2.4, 2.4]$. The third coordinate is the angle between the vertical line above the pivot point and the pole which never exceeds 12° . The second and the third coordinate is the velocity of the cart and the angular velocity which can be arbitrarily large. In our simulation, the values rarely exceeded the range $[-4, 4]$ and the majority of values reside in the interval $[-2.5, 2.5]$. We use a so-called *population encoding* which encodes each parameter as excitations of a set of neurons. A hyperparameter of this encoding is the number of neurons N_i used to encode each component x_i of the parameter vector \mathbf{x} , which we choose to be the same number N for all four components. The interval $[0, 1]$ is split in N equally-sized intervals, and we refer to the left boundaries of each of these intervals as n_j , $j \in \{1, \dots, N\}$. Each of these N intervals is assigned to a neuron and the excitation of the neuron j associated to component i is given by the following exponential function:

$$f_j(x_i) = e^{\frac{1}{2a}(|\tilde{x}_i| - n_j)}. \quad (\text{E1})$$

where $|\tilde{x}_i|$ is the normalized magnitude of the component x_i . The width of this function is given by the excitation range a . The excitation range a gives rise to a second hyperparameter, which is set in terms of the ratio $\rho = a/N$ of the excitation range to the number of neurons.

The sign of the component x_i is encoded into an additional neuron that takes the value $\text{sign}(x_i)$. In the Cartpole game, we compare the performance of agents with $N = 5$ and $N = 25$ encoding neurons to agents without population encoding while fixing $\rho = 0.000001$. Additionally, we varied the ration ρ while keeping the number of encoding neurons constant $N = 25$. In Fig. 14, we see that the performance significantly increases with the use of population encoding. The best performance was achieved with an encoding neuron number of $N = 25$ and a ratio of $\rho = 0.000001$.